RSC Advances

PAPER

View Article Online
View Journal | View Issue

Cite this: *RSC Adv.*, 2026, **16**, 27319

Effective photocatalytic and antibacterial nanomembranes from a GO-grafted dapsone-incorporated chitosan/gelatin blend for enhancing the removal of toxic dyes from wastewater

Hesham Moustafa, *[ab] Fatehy M. Abdel-Haleem,[c] Mohamed H. Hemida[d] and Heba Isawi[e]

Organic dyes, such as Eriochrome Black T (EBT) and methyl green (MG), are widely used in the textile industry, leading to their accumulation in the environment. Thus, the present study aimed to synthesise functional graphene oxide-grafted dapsone (GOgD), which was incorporated into a chitosan/gelatin (CGe) blend at different dosages (10%, 20%, and 30%) for the preparation of nanomembranes. A series of techniques and tests, including FT-IR spectroscopy, XRD, Raman spectroscopy, SEM, and mechanical and antibacterial property analyses, were applied for the characterization of functional GOgD and nanomembranes. Moreover, ultraviolet and visible light irradiations were used to evaluate the photocatalytic degradation of the EBT and MG dyes. The data revealed that optimum mechanical properties were found for CGe–GOgD 20%, with a value of ~85 MPa, compared with the unfilled blend (61.35 MPa). However, the CGe–GOgD 30% nanomembrane exhibited the best photocatalytic activity for the degradation of EBT at pH 5.0 and that of MG at pH 8.0, with degradation efficiencies of 90.8% and 97.9% under visible light and 83% and 90% under UV light, respectively. The kinetics of degradation for both dyes showed pseudo-first-order kinetics. The mechanism involved the production of the highly oxidizing species $^{\bullet}OH$ and $^{\bullet}O_2^-$ upon light irradiation, which initiated the dye degradation process, generating CO_2 and H_2O as the reaction byproducts, with complete degradation until 120 min. The photocatalyst can be regenerated and reused three times, which decreases the cost of operation. The final impact on the antibacterial activities of the nanomembranes was also investigated, and the data revealed their strong antibacterial properties against *E. coli* and *S. aureus* with different inhibitory zone diameters ranging from 21 to 34 mm, as compared with the pristine matrix. In addition to the sustainable environmental benefits of the prepared CGe–GOgD 30% nanomembrane due to the degradation of harmful organic dyes, a strong antibacterial activity was observed, highlighting its wider environmental significance and promising applications in several ecological domains.

Received 4th March 2026
Accepted 6th May 2026

DOI: 10.1039/d6ra01885h

rsc.li/rsc-advances

1. Introduction

With the growth of firms and the rise of new technologies, removing toxic dyes, including organic ones, from wastewater is an important task to maintain a safe environment for humans and all biota. High amounts of organic dyes may be present in wastewater due to the rapid development by urbanization and industrialization of textiles, paper, leather, paints and food.[1–4] Because of the poor biodegradability and toxicity of some of these dyes, and with continuous industrial development, more dyes will be released to the environment, contaminating water and soil, thereby accumulating in water, soil, and living organisms and leading to pollution, eutrophication, serious health impacts, and several ecological problems.[5,6] Accordingly, various treatment approaches have been proposed and reported for the removal of organic dyes to achieve environmental sustainability, including filtration, adsorption, redox reactions, coagulation, precipitation, electrochemical treatment, and photocatalysis.[4,7–10] Photocatalytic degradation of organic dyes, as a wastewater treatment method, is advantageous in terms of

[a]*Chemical Metrology Division, National Institute of Standards (NIS), Tersa Street, El Haram, P.O. Box 136, Giza 12211, Giza, Egypt. E-mail: hesham.moustafa21@gmail.com*

[b]*Bioanalysis Laboratory, National Institute of Standards (NIS), Tersa Street, El Haram, P.O. Box 136, Giza, 12211, Egypt*

[c]*Department of Chemistry, College of Science, Imam Mohammad Ibn Saud Islamic University (IMSIU), Riyadh, 11623, Saudi Arabia*

[d]*Department of Agricultural Engineering, Faculty of Agriculture, Cairo University, Giza, Egypt*

[e]*Water Treatment and Desalination Unit, Hydrogeochemistry Department, Water Resources and Desert Soils Division, Desert Research Center, P.O.B. 11753, Cairo, Egypt*

its sustainability, production of minimal and non-toxic by-products, eco-friendliness, mild operation conditions, energy economy, and catalyst reusability that lowers the operation cost.[11–15] The use of dopants will enhance the photocatalytic efficiency and increase the versatility of the methods for the degradation of more organic dyes.[16] Eriochrome Black T (EBT) and methyl green (MG) are used as examples of industrial textile organic dyes in this work because of their harmful impact on human health and environment, causing cellular toxicity, carcinogenicity, mutagenic problems, irritation, allergic reactions, and organ damage in humans and affecting the aquatic systems (*i.e.*, fish and algae), ecosystem distribution, soil, and plants in the environment.[17,18]

Two-dimensional graphene oxide (2D-GO) nanoplatelets have a unique honeycomb structure with a large specific surface area. The 2D-GO sheets possess reactive oxygenated sites, including carboxylic, hydroxyl, and epoxy groups, which make them highly electrically conductive materials to be used in humidity sensors.[19,20] Nevertheless, their hydrophilicity forms a significant barrier to their compounding in polymer matrices, thereby restricting their use as a reinforcement for fabricating nanomembranes for water treatment. Thus, 2D-GO nanoplatelets were grafted with hydrophobic dapsone in this study for enhancing a variety of GO properties, including hydrophobic, mechanical, antimicrobial, and photocatalytic properties. Dapsone (D) is an antibiotic medication of the sulfonamide family, which was used effectively as an antimicrobial and anti-inflammatory agent for the treatment of different diseases,[21,22] such as malaria, actinomycetoma, *Pneumocystis jirovecii* pneumonia in HIV-infected patients, leprosy, and other skin infections.[23,24] Moreover, D has a unique structure, which facilitates its modification with different polymers (polyvinyl alcohol and polyvinyl chloride) through the formation of new bonds with the amine groups, for polymer grafting and the formation of new sustainable composites or membranes.[25,26] D was also reported to interact through hydrogen bonding for the modification of the composite.[25] In some cases, D can be utilized in the decoration of certain nanoparticles to dominate their aggregations in the polymer matrices.[27] Consequently, derivatives of D and its sustainable composites were applied in different fields for improving photocatalytic and antimicrobial activities, wastewater treatment, and active food packaging purposes, without any harmful effects on humans.[21,27,28]

Gelatin (Ge) is a biocompatible, natural, water-soluble biopolymer that can be extracted simply *via* partial hydrolysis of collagen.[29] Ge has an interesting amino acid sequence, including hydroxyproline, proline, and glycine, which facilitates the construction of flexible films; it can be fashioned into other shapes, such as membranes, hydrogels, bio-aerogels and scaffolds.[30,31] However, the high hydrophilicity and antimicrobial inactivity limit its use, especially in water purification applications. Chitosan (C) is another natural linear polysaccharide biopolymer that can be synthesized chemically from chitin through deacetylation; C is characterized by its sustainability, biocompatibility, non-toxicity, biodegradability, and ability to form films.[32,33] C is soluble in water at an acidic pH due to the amino group protonation, which allows its interaction with negatively charged species, bacteria or biological pollutants.[29] It was reported that both C and Ge are sustainable water treatment agents and good barrier properties for some gases, such as CO_2 and O_2; however, both biopolymers exhibited limited mechanical and water barrier properties, due to their hydrophilic nature.[29,30] For improving these properties, both Ge and C are blended, forming a composite film (CGe) with synergistic properties from both polymers; different interactions can exist between C and Ge, such as hydrogen bonding and electrostatic interactions between the positively charged amino group of C and the negatively charged carboxylate of Ge under appropriate pH conditions. The formed CGe blend is advantageous in terms of improved mechanical strength, water resistance, compatibility, environmental friendliness, high adsorption capacity for pollutants, tunable porosity and flexibility.[30,33] However, the CGe blend may still exhibit some problems, which may restrict its use in environmental water treatment. In real-world applications, the mechanical properties are still limited by the poor mechanical and dimensional stability and low physical strength of the CGe blend, which causes its rupture and deformation, affecting the durability; this requires replacement of the CGe blend or its membrane in water treatment systems.[34]

To overcome these drawbacks and improve the photocatalytic and antimicrobial properties, the CGe blend should be used for wastewater treatment. Different substances were immobilized in the blend matrix in order to improve the usability and recovery of the photocatalytic membrane, preventing secondary pollution caused by nanomaterials.[35] For instance, potassium pyroantimonate and genipin were added to the CGe blend as a double crosslinker, which improved the contact angle, hydrophobicity, thermal stability, and the membrane mechanical properties to facilitate its use in wastewater treatments.[36] However, double crosslinking is a complex process, besides using toxic substances, such as potassium pyroantimonate, which is the opposing principle of sustainability. Another report included the incorporation of zirconium(IV) selenophosphate into CGe to form a nanocomposite ion exchanger.[37] Although this method was effective in water treatment, it included several preparation steps for the nanocomposite ion-exchanger, in addition to the use of harmful chemicals. Sethi *et al.*[1] reported the loading of CGe hydrogels with ZnO nanoparticles for the photocatalytic degradation of Congo red dye. This method resulted in a removal efficiency of 90%, but included several hydrogel preparation steps, and used maleic anhydride as a crosslinker and ammonium persulfate as an initiator. Additionally, Queirós *et al.* reported that.

In this work, the photocatalytic and antimicrobial properties of the CGe blend were improved by incorporating sustainable and environmentally benign substances; D was used for the grafting of GO, and the functional nanocomposite (GOgD) was incorporated with different dosages in the CGe blend, and used for the preparation of sustainable nanomembranes, that can be used several times for the removal of the toxic organic dyes, including EBT and MG from wastewater, without the need for harmful chemical use. The synthesis of GOgD and its incorporation into the CGe blend at different dosages highlighted the significance of resource efficiency by using existing materials

for the preparation of the catalyst, thereby lowering costs. This research also provides an ecofriendly solution for EBT and MG removal by photodegradation, boosting long-term performance and optimizing resource utilization, which confirms the sustainability concept. Additionally, the CGe–GOgD 30% nanomembrane was also applied to an industrial real wastewater sample.

2. Materials and methods

2.1. Materials

The off-white chitosan (C) with ≥85% DA in the powder phase of $M_w \approx 413$ was offered by Merck, Germany. Gelatin (Ge) powder was obtained from LANXESS, India. The 2D-GO nanolayers used as a reinforcing material were synthesized from graphite flakes using the Hammers route, as previously reported in the literature.[20] Dapsone (D), also known as 4,4-diaminodiphenyl sulfone, with a purity of 98%, and used as a modifier, was bought from Alfa Aesar, USA. Merck provided the cationic and anionic dyes, including Eriochrome Black T (EBT) and Methyl Green (MG). The MG and EBT were utilized as examples of organic contaminants in the photocatalytic procedures. A pH meter (3510, Jenway, UK) was used to adjust the pH with HCl (30%) and NaOH (98%), supplied by El-Motaheda. Deionized water (DIW) was used during the experiments.

2.2. Synthesis of GOgD nanoplatelets

The surface grafting of GO nanolayers with dapsone (D) was performed using an assisted-tip sonication approach (Fig. 1). First, 1 g of GO was dispersed in 100 mL DIW in an ultrasonic

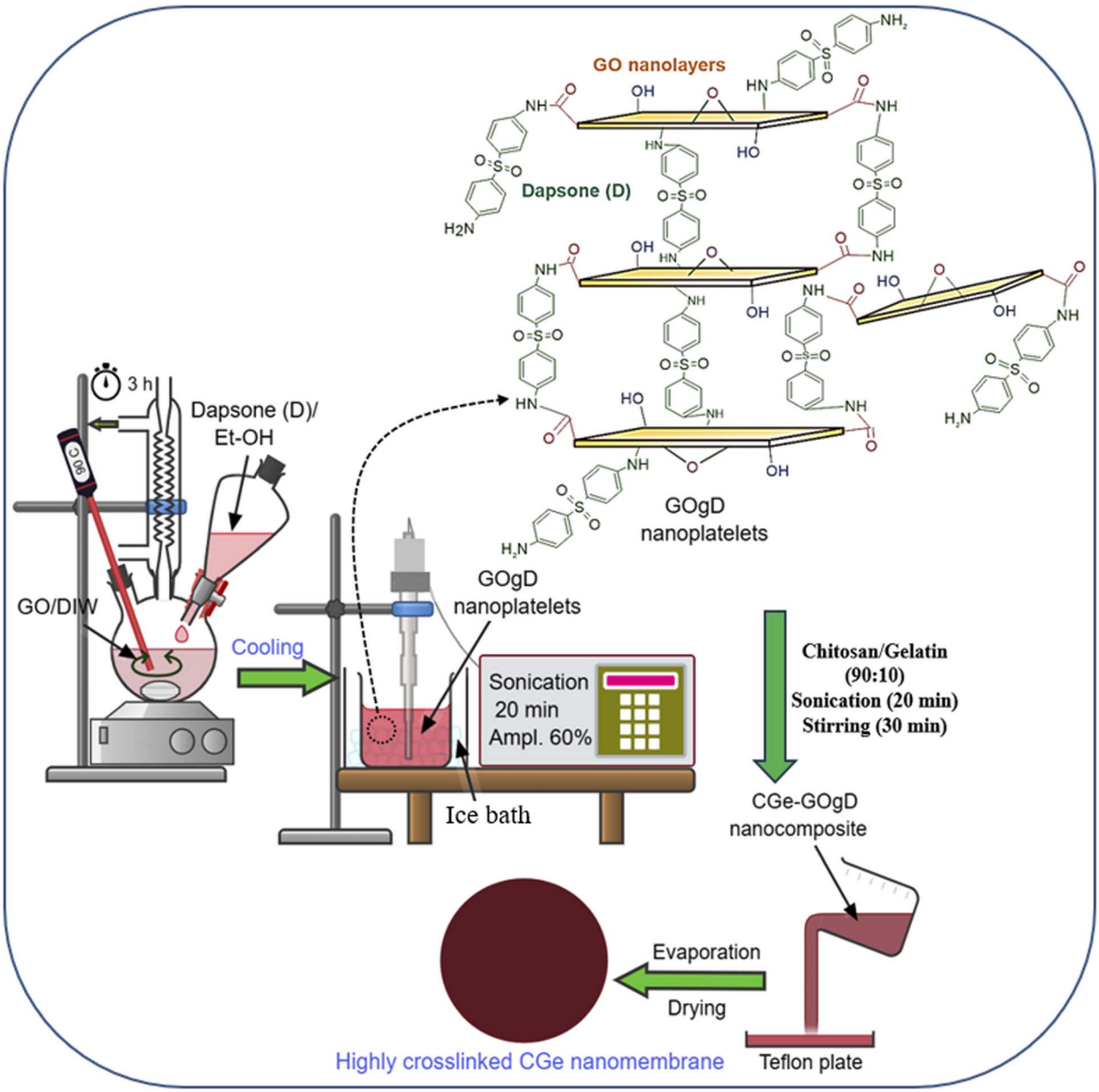

Fig. 1 Schematic of the synthesis of the GOgD nanoplatelets and CGe nanomembranes.

bath for 30 min under ambient conditions. In parallel, 0.5 g of D was completely dissolved in 100 mL of EtOH (99%) and added to the GO solution. Both solutions were transferred into a round-bottom flask fitted with a condenser, stirred for 3 h at 80–90 °C, and then cooled to room temperature. Next, the admixture was subjected to probe-sonication for 20 min at 60% amplitude, while maintaining it in an ice bath to avoid liquid evaporation. The obtained GOgD was characterized by FT-IR spectroscopy, XRD, and Raman spectra to confirm the grafting operation (Fig. 1).

2.3. Fabrication of nanomembranes

The nanomembrane-based CGe blend with variable dosages of GOgD was prepared using a solvent-casting approach. In brief, 4 g of C was dissolved in 200 mL of acetic acid solution (1%: 1 mL of glacial acetic acid diluted to 100 mL DIW) under stirring at room temperature until the C polymer was completely dissolved. This was followed by filtration of the solution to remove any impurities. Correspondingly, 5 g Ge polymer was dispersed in 50 mL of DIW under stirring, and the temperature was then increased to 50 °C for 1 h to obtain a clear solution. Subsequently, both biodegradable polymers (CGe) were blended at a volume proportion (90 : 10) under agitation for 25 min at ambient temperature, before incorporating with the reinforcement. This proportion was selected as optimal for nanomembrane fabrication, as described elsewhere.[38] To prepare the nanomembranes, three variable proportions (*i.e.*, 10, 20, and 30 v%) were applied and individually mixed with the CGe blend, followed by the addition of 3% of PEG as a plasticizer. After that, each mixture was sonicated for 20 min and then kept under agitation for 30 min to ensure better dispersibility of GOgD in the CGe matrix. At the end, each mixture was poured into Teflon plates and left for 7 days in a room temperature for liquid evaporation. After drying, the membrane films were peeled from Teflon plates, followed by further drying in an oven at 40–50 °C for 3 h. Moreover, the CGe blank was prepared under the same conditions for comparison. The fabricated nanomembranes were labelled based on the quantity of GOgD in the nanomembranes as CGe blank, CGe–GOgD 10%, CGe–GOgD 20%, and CGe–GOgD 30%.

2.4. Characterization of nanoplatelets

2.4.1. XRD and FT-IR spectroscopy analysis. A Bruker-AXS D8 Ascertain Diffractometer equipped with a monochromator and a Cu Kα radiation source (35 kV, 30 mA, and $\lambda = 1.15418$ Å) was used for X-ray diffraction to study the structure of pure GO, GOgD, CGe blend, and their loaded nanomembranes with varying dosages of GOgD nanoplatelets. The data were measured over a 2θ range from 5° to 75° with a step size of 0.05 at a sampling width of 0.011°.[39] Additionally, the functional properties of GO and modified GOgD were investigated using a PerkinElmer Spectrum100 FT-IR spectrometer in the ATR mode. The spectral range for GO and GOgD nanoplatelets was examined from 4000 cm^{-1} to 400 cm^{-1} with a resolution of 4 cm^{-1} and 64 scans.

2.4.2. Raman spectra. The structural and chemical changes between the functional properties of pure GO and GOgD nanoplatelets were investigated using a confocal Raman microscope (model: Horiba LabRam HR evolution Raman Spectroscopy, France) equipped with a CapuR laser at a wavenumber of 532 nm.

2.5. Nanomembrane characterizations

2.5.1. SEM analysis. The biocompatibility and dispersion quality of GOgD nanoplatelets into the CGe matrices were investigated using a scanning electron microscope (SEM, QUANTA 3D 200i). The fractured cross-section surfaces were coated with a thin gold layer before SEM observations to prevent any electrostatic charging during the visualization. The acceleration voltage was 5–10 kV.[40]

2.5.2. Mechanical testing. An Instron 34SC-5 Universal Tensile testing machine, UK, with a load cell of 5 kN, was used to perform the mechanical properties with a crosshead speed of 100 mm min^{-1}, according to ASTM D 882-18. All samples were conducted under normal conditions at 23 °C ± 2 °C and 50% ± 5% relative humidity. The mean value was taken from five parallel trials for each sheet.[41]

2.5.3. Water contact angle measurements. The hydrophilicity of the fabricated nanomembranes was estimated using a water contact angle (WCA) (Cam-plus Micro, Tantec Inc., US), in which a view from the side photograph was recorded after 3 μL of dewdrops of DIW were deposited onto the membrane surface for 10 seconds. The mean value was taken from at least three trials for each membrane.

2.5.4. Assessment of photocatalytic performances. The photocatalytic activity of the prepared nanomembranes (CGe–GOgD 10%, 20%, and 30%) was evaluated through the degradation of aqueous solutions of MG and EBT, representing cationic and anionic dyes, respectively. Irradiation was carried out under two light sources: (i) UV light using a Sylvania UVA lamp (F40W/2FT/T12/BL368), and (ii) visible light using a 500 W halogen lamp equipped with a 420 nm cutoff filter to eliminate UV contributions. The light source was positioned at a fixed distance of 40 cm above the reaction mixture to ensure consistent irradiation conditions. All experiments were conducted under identical geometric conditions to ensure reproducibility. For each experiment, 0.2 g of nanomembrane was immersed in 30 mL of dye solution. The photocatalytic degradation performance was systematically investigated by varying key operational parameters, including irradiation time, solution pH, and initial dye concentration. The concentration changes of MG and EBT were monitored using a UV-visible spectrophotometer. All experiments were conducted at ambient temperature (25 °C ± 2 °C), and no significant temperature increase was observed during irradiation, indicating that the degradation process is primarily attributed to photocatalytic activity rather than thermal effects. Before the experiment, the mixture was vigorously stirred for 30 min in the dark to ascertain the dye's adsorption/desorption equilibrium amount and attain sufficient distribution uniformity. A known quantity of the nanomembranes (adsorbent) was combined

with a 30 mL solution of each color for each experiment. The batch mode tests were conducted as follows: at room temperature, 0.2 g of nanomembranes and 30 mL of dye were spun for 180 min at a steady 130 rpm to get the desired concentration. A 1000 ppm stock solution was prepared and diluted for each dye. Solutions of HCl or NaOH (0.1 M) were used to adjust the pH between 2 and 10 in order to investigate the pH influence. The maximum absorbance (λ_{max}) of MG and EBT dyes was measured at proper wavelengths, which are 633 and 530 nm, respectively. After each experiment was completed under similar conditions, the average values were calculated. MG and EBT dyes at 1–100 mg L^{-1} were used for kinetics testing, whilst adsorption isotherm investigations were conducted using 10 mg L^{-1} of each dye at 25 °C. A UV-visible spectrophotometer was used to measure the residual dye concentration. The following formulas were used to calculate the adsorbent's removal efficacy (R%) and absorption capacity (Q_e), which represented the time interval between time t (q_t) and its stability time q_e: V (L) and m (g L^{-1}) are the volume of the solution containing the dye and the adsorbent's dosage, respectively, and C_0 and C_t are the starting and stability dosages at time t (mg L^{-1}).

$$R\% = \frac{(C_0 - C_t)}{C_0} \times 100, \quad (1)$$

$$Q_e = \frac{(C_0 - C_t) \times V}{m}. \quad (2)$$

2.5.5. Recyclability and regeneration of the nanomembranes. Stability is one of the most important prerequisites for photocatalysis.[42,43] The recyclability of the CGe–GOgD 30% nanomembrane was evaluated using repeated degradation cycles for MG and EBT dyes. The photocatalyst was cleaned with ethanol and DI water after each cycle, dried in an oven for 60 minutes at 50 °C, and then used again for the photodegradation of dyes. The same technique was used to evaluate the regenerated dyes and their adsorption and desorption cycles. The regeneration efficacy (RE%) was computed using the following formula. The following formula was used to determine the regeneration efficacy (RE%), where q_{de} is the amount of each dye that was desorbed and q_{ad} is the amount of each dye that was adsorbed during the loading procedure.

$$RE\% = \frac{q_{de}}{q_{ad}} \times 100. \quad (3)$$

2.5.6. Application studies using the CGe–GOgD 30% nanomembrane for a natural contaminated wastewater sample. The CGe–GOgD 30% nanomembrane was applied to a natural wastewater sample that was taken from the dye basin of a textile factory in 10th Ramadan City, Cairo, Egypt. Various samples were collected at intervals of 10 min up to 120 min to determine the residual dye concentration. Using a UV/visible spectrophotometer (Unicam, model 300, England) and the absorbance (nm) method, the residual dye concentration was determined in the solutions. A halogen lamp (500 W, connected *via* a 420 nm stalling filter) was used to degrade the wastewater sample under visible light. The following equation, where A_i and A_f represent the dye solution's initial and final absorbance, respectively, was used to assess the dye degradation efficacy. Each treatment was used twice in this investigation, and each sample's absorbance was tested three times. The results are averaged in the figures and tables.

$$\text{Degradation efficiency } (\%) = \frac{A_i - A_f}{A_i} \times 100. \quad (4)$$

Calculations for the entire chemical analysis were done, both before and after the photocatalytic breakdown. The EC and pH were measured using electrical conductivity (EC) meters (model Orion 150 A^+). The total organic carbon (TOC) was calculated using titrimetric analysis. The trace metal ions were estimated using an Inductively Coupled Argon Plasma (ICP) 6500 Duo spectrophotometer (Unicom, UK).

2.5.7. Antibacterial assays. The CompactDry™ TCR agar diffusion disks, which were offered by Nissui Pharmaceutical Co., Japan, were used as vegetated media for *Escherichia coli* (*E. coli*, G^{-ve} bacteria) and *Staphylococcus aureus* (*S. aureus*, G^{+ve} bacteria). Both bacteria were individually spread on the media using the agar disk-diffusion method. The nanomembrane specimens (approximately 10 × 10 × 1.5 mm in size) were dried in a room temperature under sterilized conditions prior to the experiment and then placed on top of the media surface seeded with selected microbes, followed by incubation for 24 h at 37 °C.[44,45] The microbes were cultivated around the sample after the incubation time, and the inhibition zone diameter (IZD) was recorded.

3. Results and discussion

3.1. Characterization of grafted GogD and its nanomembranes

The FT-IR spectroscopy, XRD, and Raman spectra were used to investigate the chemical structure and crystallinity of grafted GogD compared to pure GO, as displayed in Fig. 2(a–c). The FT-IR spectra of pure GO typically illustrated the main characteristic bands at ~3402 cm^{-1}, 1718 cm^{-1}, and 1065 cm^{-1}, corresponding to –OH stretching, carbonyl (–C═O), and epoxy (–C–O–C–) groups, respectively, which proved that the GO possessed strong oxygenated layers.[46] After grafting, a broad band was observed in the region 3416–3210 cm^{-1}, which was assigned to the stretching of –OH and –NH groups[47] (Fig. 2(a)). It was also found that a slight shift occurred for carbonyl to a lower wavenumber (1706 cm^{-1}), with the appearance of a strong band at ~1601 cm^{-1}, which was assigned to the formation of the amide (–CO–NH–) group in GogD.[19,48] Meanwhile, the increase in –C–O– and –C–N– bands after the grafting process was also noticed.[19] All of them confirmed that the grafting of GO by dapsone (D) had occurred. These data were also supported by XRD patterns. It can be observed from Fig. 2(b) that a sharp diffraction peak appeared at $2\theta \approx 11.98°$ (001) for pure GO, indicating the crystal structure of the material, which confirms its nanoscale structure. As the grafting of GO by D was done, a large shift in the diffraction peak of the basal plane (d_{001}) to a lower angle, $2\theta \approx 8.21°$, was observed with a reduction in peak

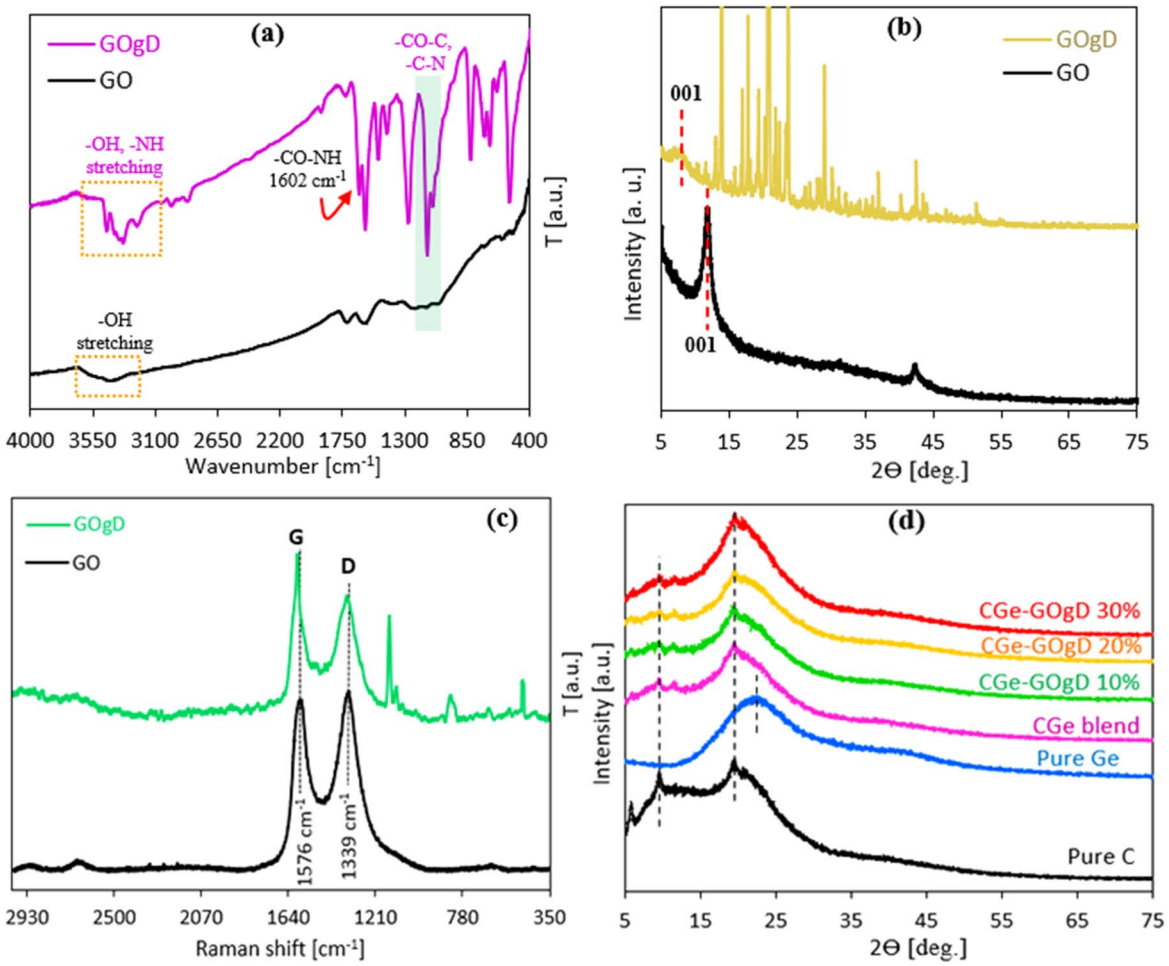

Fig. 2 (a) FT-IR spectra, (b) XRD patterns, and (c) Raman spectra of pure GO and the modified GOgD. (d) XRD patterns of the nanomembranes compared with pure C and Ge.

intensity compared to pure GO (*i.e.*, $2\theta \approx 11.98°$). Furthermore, it was noticed that the *d*-spacing distance was increased from 7.41 Å in the case of GO to 9.80 Å in the case of GogD, leading to the swelling of the GO interlayers, which facilitates the polymer chains to penetrate between the GO nanolayers for getting exfoliate or intercalate matrices. Similar findings were reported elsewhere[49] when GO was functionalized with the antitumor drug methotrexate and folic acid. In addition, more in-depth information about the changes and functional interactions in GogD was supported by Raman spectra, as depicted in Fig. 2(c). It was found that two sharp and massive bands were observed at ~1339 cm^{-1} and ~1576 cm^{-1} in the Raman region, corresponding to D (sp^3 C atoms) and G (sp^2 C atoms) for pure GO, respectively.[19] These bands appeared at the largest intensities because of the conjugation of the carbon–carbon double bonds of GO.[50] After GO grafting, a little shift in both D and G bands was noticed to a higher wavenumber of ~1345.30 cm^{-1} for the D band and 1593.70 cm^{-1} for the G band, compared to pure GO. Simultaneously, the peak intensities for both bands were also reduced. All of them were suggesting that strong functional interactions of GO and dapsone were achieved. This finding aligned with FT-IR spectra and XRD patterns, as well as with that published elsewhere,[51] in which the slight shift of the G band was due to the doping changes of the graphene plane, when GO was modified by ammonia to obtain GO-NH_3. Furthermore, Fig. 2(d) demonstrates the XRD patterns for the casted nanomembranes, in which two major diffraction peaks appeared at $2\theta \approx 10.35°$ and 19.76° for virgin C, suggesting its semi-crystalline structure. An extensive diffraction peak located at $2\theta \approx 22.40°$ was noticed for the amorphous structure of virgin Ge. When Ge was blended with C, the diffraction peak of both polymers was centered at $2\theta \approx 19.13°$ with a little reduction in the peak intensities of the blend compared to that of virgin C. This comportment may be attributed to the better miscibility between both polymers through the interactions of functional sites of the C–Ge blend matrix. Moreover, upon the integration of variable contents of GogD into the Cge matrix, the intensities of these peaks were clearly reduced, particularly up to 20% loading, suggesting that better nanofiller distribution and wettability between the constituents were achieved. This finding was aligned with that obtained by SEM observations and mechanical testing.

3.2. SEM analysis

SEM micrographs highlighted the miscibility and dispersibility of the hybrid GO nanoplatelets at varying dosages within the Cge

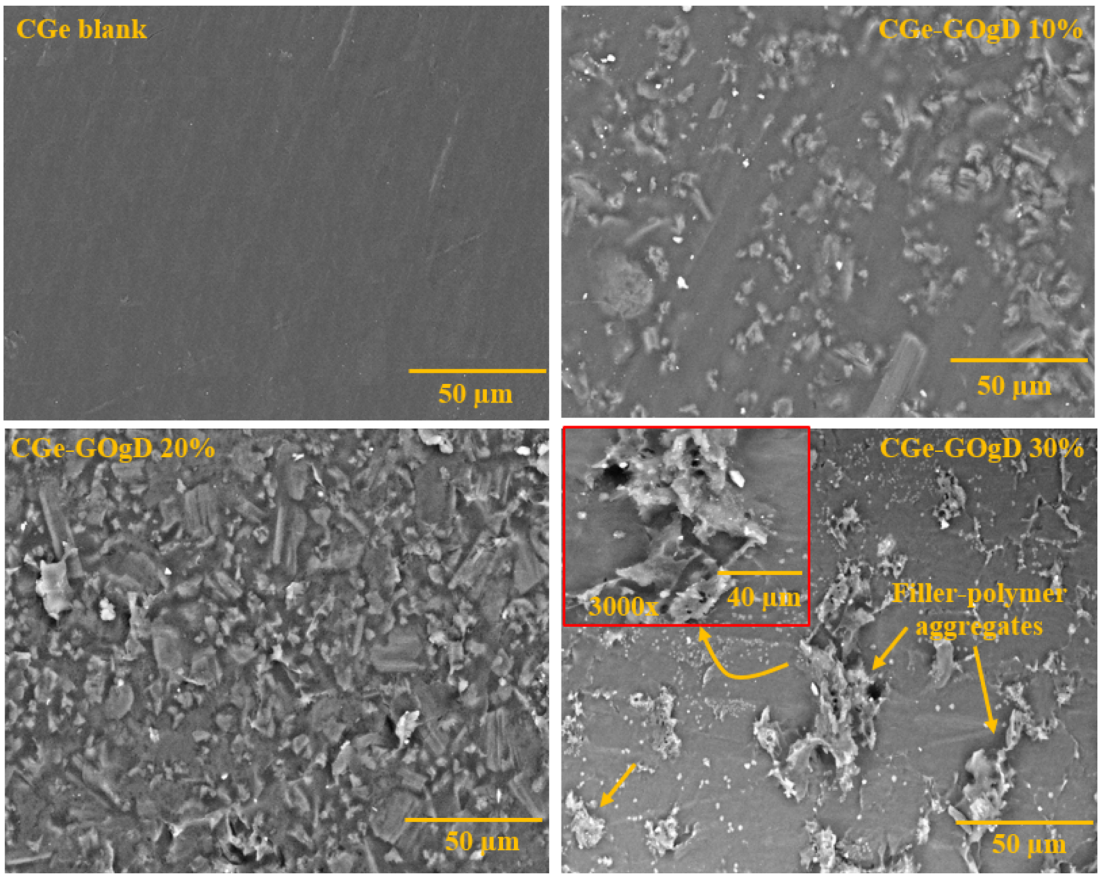

Fig. 3 SEM micrographs of the CGe blank and the nanomembranes containing various proportions of the GOgD nanoplatelets under a magnification of 1500× and additionally under 3000× for the 30% sample.

blend, as illustrated in Fig. 3. The morphology of the fractured surface of the Cge blank was quite uniform, without any halos or cracks, suggesting good compatibility between the two water-soluble biopolymers. When 10% or 20% GogD was incorporated into the matrix, a rough surface was noticed, but GogD nanoplatelets appeared to be miscible and more dispersed inside the matrix, with free voids or halos. This may be due to better nanofiller–matrix interactions resulting from the penetration of polymer chains between the grafted GO layers, which occurred due to interlayer expansion. This was leading to further functional site interfacial bonding, which may be driven to the formation of intercalated or exfoliated structures.[19] However, poor dispersion with a phase-separation (immiscibility) was noticed throughout the matrix with further addition of GogD at 30%, which may be due to nanofiller aggregation, inducing interfacial debonding between the components, thereby reducing the tensile strength. This finding is absolutely consistent with that reported in the mechanical testing.

3.3. Mechanical testing

The mechanical properties, including tensile strength (T.S.) and strain at rupture (strain%), of nanomembranes are shown in Fig. 4, and compared with the unfilled blank (Cge). These properties could play a substantial role in mitigating the predicted risk associated with the membrane material during the adsorption process, thereby leading to a prolonged product shelf-life. The data showed that the unfilled membrane (Cge) had a T.S. of ~61.35 MPa and a strain of 44.6%. Similar trends were reported elsewhere.[52] For nanomembranes, a significant increase in the T.S. properties was observed, and their values jumped to ~74.70 MPa and 84.63 MPa with 10% and 20% of GogD contents, respectively. The best enhancement in T.S. values was apparently due to the strong chemical interactions between the constituents, which contribute to the good GogD distribution and interfacial bonding between the functional sites of nanoplatelets and Cge matrix.[53] Contrarily, upon further incorporation of GogD into the matrix (*i.e.*, 30%), the T.S. began to decrease obviously to ~77.50 MPa, due to the nanofiller aggregates, which created clusters and voids along the Cge matrix, resulting in the premature rupture of the blend matrix. In spite of the tensile properties of the CGe–GOgD 30% nanomembrane being reduced at a higher nanofiller proportion (*i.e.*, 30%), its value was still substantially higher than that for unfilled Cge (*i.e.*, 61.35 MPa). Additionally, the percentage of strain was also gradually reduced with the increasing GogD quantity, due to the enhancement of the reinforcing agent impact. It can be rounded up that the best achievement in tensile properties was observed for the CGe–GOgD 20% nanomembrane.

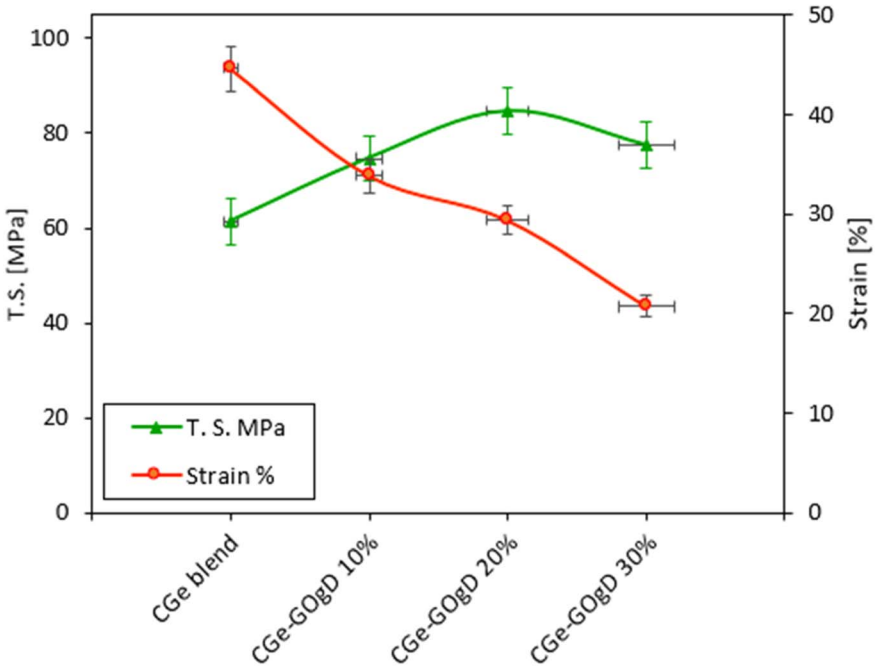

Fig. 4 Tensile properties of unfilled CGe and the nanomembranes with different dosages of GOgD.

3.4. WCA measurements

To stop liquid from entering the holes, the membrane surface must have low wettability. As shown in Fig. 5, the results showed that the nanomembrane's contact angle values decreased as the ratio of GogD-to-polymer increased from 10% to 30%. For Cge blank, CGe–GOgD 10%, CGe–GOgD 20%, and CGe–GOgD 30% nanomembranes, the corresponding values were 76.2° ± 1.5°, 72.4° ± 1.3°, 59.5° ± 1.6°, and 54.5° ± 1.2°, indicating an increase in the hydrophilicity of the material. It was discovered that the addition of functional groups involving oxygen results in a decrease in WCA value and an increase in surface energy, which improves the wettability. The hydrophilicity of the membranes was increased by the addition of GO grafted with dapsone (GogD), which caused the contact angle to gradually decrease from 76.2° ± 1.5° for the pure Cge membrane to 54.5° ± 1.2° with the increasing GogD loading (30%). The numerous polar functional groups (*i.e.*, –OH and –NH_2) of GogD, which increase surface affinity toward water, were responsible for this behavior.

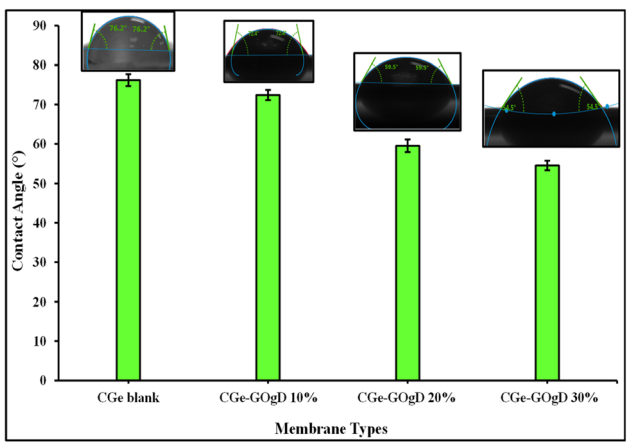

Fig. 5 Water contact angle assessment for the CGe blank, CGe–GOgD 10%, CGe–GOgD 20%, and CGe–GOgD 30% nanomembranes.

3.5. Photocatalytic performance

3.5.1. Influence of UV/visible light radiation on the photocatalytic activity of nanomembranes. Fig. 6(b) illustrates the photocatalytic degradation of MG and EBT dyes under UV and visible light radiation using Cge blank, CGe–GOgD 10%, CGe–GOgD 20%, and CGe–GOgD 30% nanomembranes, without the need for chemicals, confirming the sustainability and environmental safety of the proposed method. The results showed that increasing the grafting ratio for MG and EBT dyes and irradiation sources significantly improved the photocatalytic degradation performance. Reasonable photocatalytic degradation efficiencies of 63.5% for EBT and 65% for MG were demonstrated by the Cge blank. With the addition of 10% GogD to the Cge matrix, the degradation efficiency for EBT and MG increased to 69% and 74% in the case of visible light and to 66% and 70% in the case of UV light, respectively. When increasing the GogD content to 20% and 30%, a significant change in the degradation efficiencies for EBT and MG was observed. Under visible light, the CGe–GOgD 20% nanomembrane achieved higher degradation efficiencies of 84.4% and 87% for EBT and MG, respectively; under UV light, it demonstrated 77% and 83%. For CGe–GOgD 30%, under visible light, it achieved much higher removal efficiencies of 90.8% and 97.9% for EBT and MG, respectively, and 83% and 90% under UV light. Therefore, the photocatalytic degradation existed in the following order: CGe–GOgD 30% > CGe–GOgD 20% > CGe–GOgD 10% > Cge blank, when irradiated with UV or visible light (Fig. 6). Although

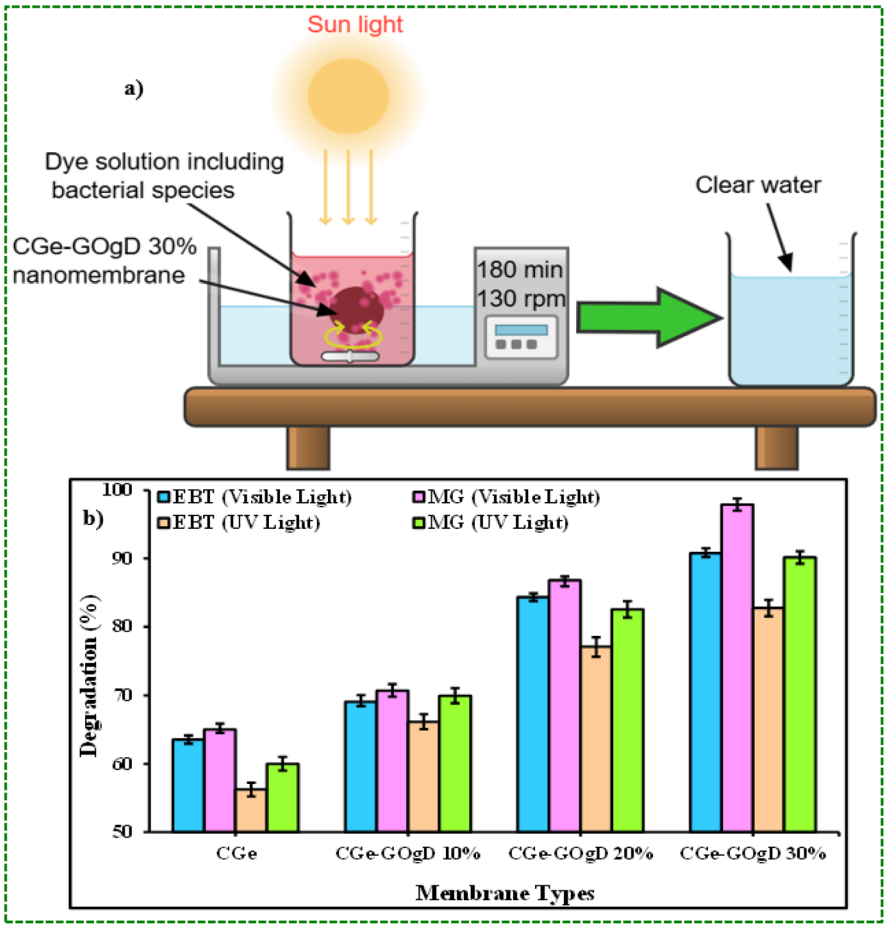

Fig. 6 (a) Schematic of the photocatalytic degradation method. (b) Effect of the photocatalytic degradation of the MG and EBT dyes using the pure CGe, CGe–GOgD 10%, CGe–GOgD 20%, and CGe–GOgD 30% nanomembranes under UV and visible light irradiation at room temperature using 5 mg L^{-1} of each dye for a contact time of 180 min, nanomembrane dose = 7 g L^{-1}, shaking speed = 130 rpm, and pH = 5 for EBT and pH = 8 for MG.

photocatalytic degradation was also aided by UV irradiation, the results were consistently less effective than those obtained with visible light radiation. The natural sensitivity of GO-grafted dapsone to visible light radiation may be the cause of this higher performance, as it facilitates the removal of responsibilities and outspreads light absorption into the visible area. However, UV exposure tends to accelerate electron/hole recombination and may partially disrupt the stability of the Cge matrix, hence controlling the production of radicals. Additionally, more reactive oxygen species ($^{\bullet}OH$ and $^{\bullet}O_2^-$) are produced as a result of the enhanced visible light absorption, which promotes more efficient dye decomposition. Additionally, due to stronger electrostatic bonds formed among the cationic MG molecules and the negatively charged GO surface, which promote adsorption and the ensuing photocatalytic reactions, the cationic MG dyes demonstrated higher photocatalytic degradation efficacies than the anionic EBT dye in every situation. Because of its π–π* (bonding–antibonding) transitions, oxygenated groups allow visible light absorption, and the operational band gap is smaller than that of typical UV photocatalysts, GO plays a better role in photocatalytic activity under visible light photocatalysis. Additionally, it functions as an electron transport, reducing e^-/h^+ recombination. Because both GO and D have conjugated structures, the addition of GogD may affect the photocatalytic behavior under visible light. Specifically, D has sulfone groups ($-SO_2^-$) and aromatic rings, which are known to show UV absorption linked to π → π transitions and the associated photophysical reactions.[54] When incorporated into the Cge matrix, these structural elements may promote photo-induced processes and contribute to light–matter interactions. Therefore, rather than a direct sensitization mechanism, the enhanced photocatalytic activity seen for the Cge–GogD 30% nanomembrane under visible light can be attributed to the combined effect of GO and GogD inclusion. Furthermore, the membrane matrix's polymeric structure restricts excessive photocatalytic activity when exposed to UV light, leading to a more regulated degradation behavior. Bhattacharya *et al.* claimed that π → π electronic transitions within the conjugated aromatic structure of dapsone are responsible for its characteristic absorption maxima at around 261 and 295 nm.[55] These features demonstrate that, when incorporated into the composite system, they can contribute to light–matter

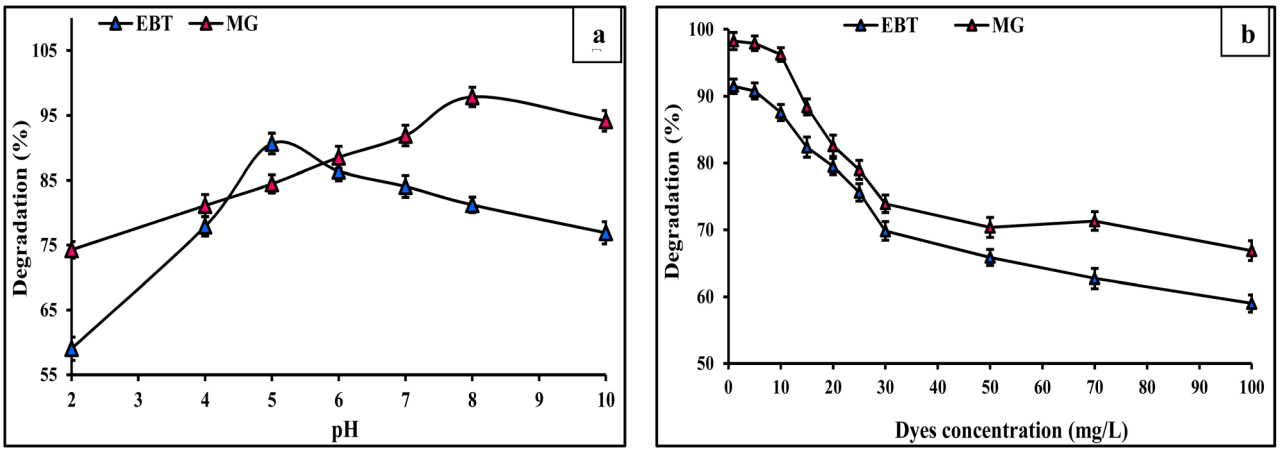

Fig. 7 (a) Effect of pH on the photocatalytic degradation using 5 mg L^{-1} of each dye. (b) Effect of the MG and EBT dye concentrations on the nanomembrane photocatalytic degradation performance at 25 °C, with the dye concentration ranging from 1 to 100 mg L^{-1} at a contact time of 180 min, pH = 5 for EBT and pH = 8 for MG at room temperature, and under visible light exposure using the CGe–GOgD 30% nanomembrane.

interactions and undergo electronic excitation under UV irradiation.

3.5.2. Influence of pH. The initial pH of the solution has a significant impact on the photocatalytic degradation of EBT and MG dyes utilizing the CGe–GOgD 30% nanomembrane under visible light irradiation (Fig. 7(a)). Due to the excessive protonation of surface functional groups (–NH_2, –OH, and –COOH) on GogD and the Cge matrix, which inhibits dye adsorption and lowers the production of reactive oxygen species under visible light, relatively low degradation efficacies for EBT and MG dyes were observed in acidic media at a lower pH of 2. Due to the enhanced electrostatic interaction between EBT as an anionic molecule and the positively charged sites of the CGe–GOgD 30% nanomembrane, the breakdown efficiency of EBT reached the maximum value at pH 5 (90.7%) as the pH increased to somewhat acidic values. Additionally, GogD facilitated the absorption of visible light and accelerated charge separation, thereby improving the generation of reactive oxygen species ($^{\bullet}OH$ and $^{\bullet}O_2^-$) that hasten the breakdown of EBT. However, the MG showed that the photocatalytic degradation efficiency increased steadily as the pH increased, peaking at pH 8 (97.9%). The GogD surface became more negatively charged in alkaline environments, which promoted robust electrostatic attraction with the cationic MG dye molecules. Moreover, increased OH availability enhanced the production of hydroxyl radicals ($^{\bullet}OH$) when exposed to visible light, which boosted the effective mineralization of MG dye.[56,57] The photocatalytic breakdown rate for EBT and MG dyes showed a modest decline at pH 10, which might be explained by partial shielding of active patches on the CGe–GOgD 30% membrane surface and excessive hydroxide ions acting as radical scavenging agents. These results demonstrated the critical role of pH-controlled surface charge and dye catalyst interactions. Generally speaking, the CGe–GOgD 30% nanomembrane exhibited excellent visible light energetic photocatalytic activity, with optimal performance occurring at pH 5 for EBT (anionic dye) and pH 8 for MG (cationic dye). These findings are consistent with the results of other research studies that used membranes based on GO nanoplatelets for photocatalytic decomposition.[40,58] This behavior is consistent with earlier studies on GO–dapsone composite membranes, where it was demonstrated that adding dapsone changed the surface charge properties of graphene oxide-based systems by protonating and deprotonating amine groups, which in turn affected pH-dependent electrostatic interactions and adsorption behavior.[59]

3.5.3. Effect of dye concentration. Using the CGe–GOgD 30% nanomembrane exposed to visible light, the impact of initial dye concentration on the photocatalytic degradation of MG and EBT was examined in (Fig. 7(b)). The device demonstrated outstanding photocatalytic efficacy at low dye concentrations (1–5 mg L^{-1}), attaining degradation efficiencies of over 98% for MG and 91% for EBT. According to the quantity of MG and EBT dye molecules in the solution, there are enough active sites and reactive oxygen species available to cause this behavior. For MG and EBT dyes, a progressive decline in degradation efficiency was noted as the initial dye concentration increased from 10 to 30 mg L^{-1}. Increased competition for adsorption sites on the CGe–GOgD 30% nanomembrane and improved light screening effects caused by higher dye loadings restricted photon penetration and reduced the production of radicals triggered by visible light. Moreover, catalytic sites may be partially blocked by the buildup of intermediate degradation products, which would further reduce the degradation efficiency.[60] The degradation efficiencies clearly declined at higher concentrations, ranging from 50 to 100 mg L^{-1}, reaching roughly 67% for MG and 59% for EBT at 100 mg L^{-1}. Due to its cationic characteristics, which result in stronger electrostatic binding with the negatively charged CGe–GOgD 30% nanomembrane surface and more effective transference of charge under visible light, facilitated by the D modifier, MG consistently demonstrated higher degradation efficiencies than EBT across the whole concentration range. These results demonstrated the potential of the CGe–GOgD 30% nanomembrane for useful wastewater treatment applications under visible light by

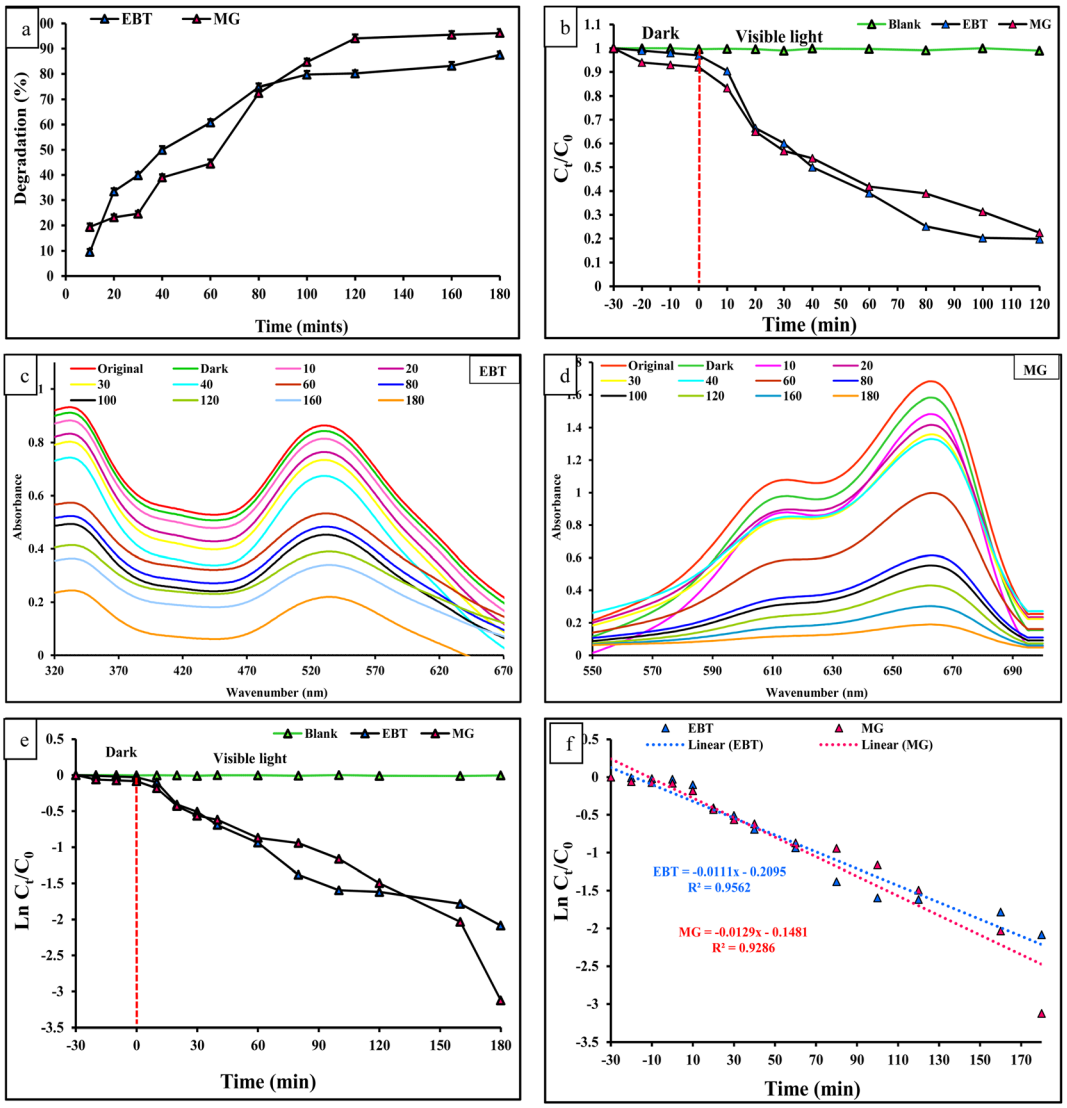

Fig. 8 (a) Photocatalytic degradation plots. (b) Effect of contact time on the degradation of the EBT and MG dyes. (c and d) UV-visible spectra. (e and f) Photocatalysis kinetics as plots of $\ln(C_t/C_0)$ of the EBT and MG dyes using the CGe–GOgD 30% nanomembrane under visible light irradiation, dye concentrations = 10 mg L^{-1}, contact time = 0–180 min, nanomembrane dose = 7 g L^{-1}, and at room temperature.

showing that it is highly effective at low to moderate dye concentrations while maintaining the reasonable photocatalytic activity even at high pollutant levels. Because of its superior e^-/h^+ pair separation rate, the rGo/NiO_x/Ag ternary system demonstrated the highest photoactivity of methylene blue dye (95%) under simulated sunshine irradiation, which aligned with that published elsewhere.[61] Additionally, Tolkou *et al.*[62] applied 1.0 g per L GO–Al to 5 mg per L humic acid (HA); 91% of the material was eliminated after 24 h, but equilibrium was nearly attained after 30 min (82% elimination).

3.5.4. Effect of contacting time and estimating adsorption kinetics. An exposure time study (1–180 min) was carried out using 10 mg L^{-1} of EBT and MG dyes at room temperature and pH values of 5 and 8, respectively. A 60 mL of each dye solution was used to soak 0.4 g of CGe–GOgD 30% nanomembrane under visible light. As shown in Fig. 8, the effect of contact time on the photocatalytic degradation of EBT and MG dyes was examined for 1 to 180 min. Using the CGe–GOgD 30% nanomembrane, the EBT and MG dyes showed quick early degradation, which was followed by a steady rate of degradation until equilibrium was reached at 180 min (Fig. 8(a)). After 180 min of exposure, the efficiency of photocatalytic degradation for EBT and MG dyes reached 87.6% and 96.2%, respectively, demonstrating that the breakdown rate increased in proportion to the longer contact duration. This suggested that the longer the contact time between the dye and the photocatalyst during the photocatalytic process under visible light, the more the degradation of the dye. The C_t/C_0 *vs.* time plot of EBT and MG dye solutions, which had initial concentrations of 10 mg L^{-1} and were broken down by the CGe–GOgD 30% membrane under ideal circumstances, was linked to visible light (Fig. 8(b)). Before irradiation, the dye's absorption/desorption isotherm

Table 1 Degradation efficiency of the EBT and MG dyes using the CGe–GOgD 30% nanomembrane under visible light irradiation, dye concentration = 10 mg L^{-1}, contact time = 0–180 min, membrane dose = 7 g L^{-1}, at room temperature and the corresponding pseudo-1st-order rate constants

	Degradation efficiency (%)		
Dye type	Dark condition after 30 min	After 180 min of light exposure	Rate constant, k (min^{-1}), of visible light exposure
EBT	6	87.7	0.0111
MG	10	96.2	0.0129

was measured by magnetically stimulating the solution in the dark for half an hour. According to Fig. 8(b), the ratio was smaller in the dark under the same experimental conditions, indicating that the self-photolysis of MG and EBT dyes can be disregarded. Additionally, it was evident that the MG and EBT dye concentrations gradually dropped until they reached equilibrium after 180 min. The inclusion of the CGe–GOgD 30% nanomembrane, which greatly enhanced the catalyst's photoactivity by reducing e^-/h^+ pair recombination and enhancing light harvesting capabilities, was credited with this exceptional result. Fig. 8(c and d) show the UV-visible spectra of 10 mg L^{-1} of MG and EBT dyes obtained at different times during the photodegradation tests using the CGe–GOgD 30% membrane under visible light irradiation. As shown in Fig. 8(c and d), the emission spectra of EBT and MG were recorded over a period of up to 180 min in the wavelength ranges of 320 to 670 nm and 550 to 700 nm, respectively. According to the plots, the primary extinction peaks of the EBT and MG dyes were located at 530

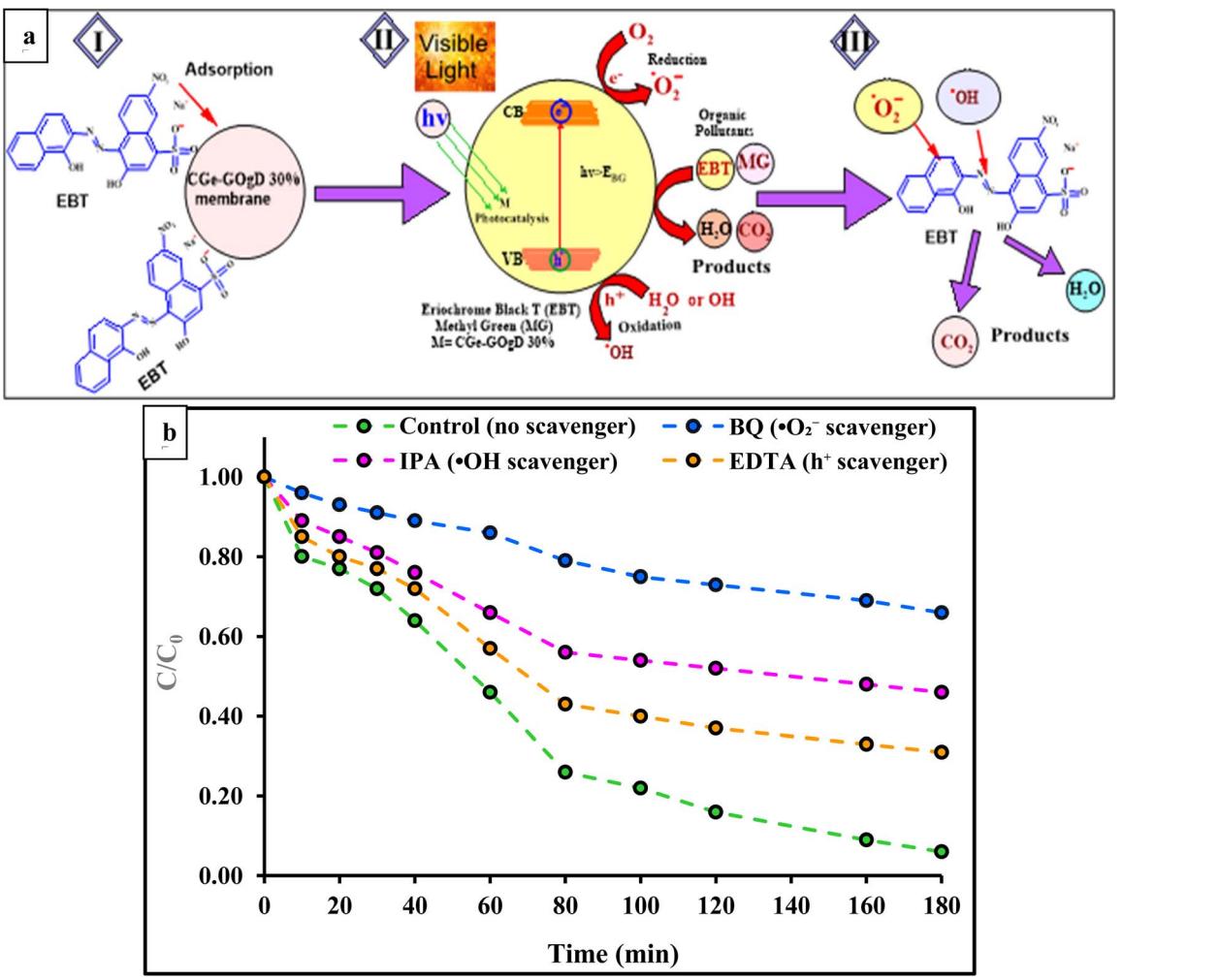

Fig. 9 (a) Schematic of the photocatalytic procedure using the CGe–GOgD 30% nanomembrane under visible light irradiation in three stages of the degradation of the EBT dye. (b) Effect of different scavengers on the photodegradation of the EBT dye after 180 min under visible light irradiation (dye concentrations = 10 mg L^{-1}, contact time = 0–180 min, membrane dose = 7 g L^{-1}, and at room temperature).

Table 2 Comparative assessment of the photocatalytic performance of the CGe–GOgD 30% nanomembrane with those reported in most recent studies

GO systems	Light source	Pollutants	Experimental conditions	Degradation efficiency (%)	Ref.
GO/ZnO/Ag composites	Under visible light irradiation	Ciprofloxacin (CIP)	20 mg per L CIP concentration, 15 mg catalyst dosage, GO/ZnO-3%/Ag-doping ratio, and pH 5	Maximum degradation rate of 82.13%	66
N–TiO_2/CuO/GO photocatalysts	Visible-light irradiation	Formaldehyde	6 h	74% degradation efficiency	67
Magnetic Fe_3O_4 nanoparticle (NP)-decorated rGO/TiO_2@MXene (RFTM) aerogel	Visible-light irradiation	Rhodamine B and tetracycline		93% degradation of RhB within 120 min and 95% degradation of TC within 30 min	68
Reduced graphene oxide laminated TiO_2–B NW composites [R(GO/TNW)]	Visible-light irradiation	RhB dye under visible light	0.05 g semiconductor and 100 min	96%	69
GO (x wt%)/TiO_2–CA hybrid membranes	Visible-light source (Xe lamp)	Methyl orange	50 mg L^{-1} of MO, 0.1 MPa pressure at room temperature, and 50 min	MO rejection high (96.6%)	70
TiO_2/GO/$CuFe_2O_4$ heterostructure photocatalyst	Under UV irradiation	Photocatalytic degradation of 17 different chlorinated pesticides (persistent organic pollutants)	At various times and different concentrations of 0.1, 0.15, and 0.05	96.5% photocatalytic removal efficiency of a typical pesticide DDE from water	71
GO–ZnO photocatalyst	Solar simulator Atlas Suntest CPS$^+$ xenon lamp (1500 W and 500 W m^{-2} intensity)	Two azole fungicides, fluconazole and voriconazole	At a catalyst dosage of 100 mg L^{-1} and treatment time of 60 min	GO–ZnO was highly effective against fluconazole, achieving 79.7% removal	72
$NiFe_2O_4$/GO/PVDF	UV	Remazol Red (RB-133)	60 min	92%	73
CGe–GOgD 30% nanomembrane	Visible light and UV light	Eriochrome Black T (EBT) and methyl green (MG)	0.2 g of membrane was immersed in 30 mL of dye solution, dye concentration = 10 mg L^{-1}, contact time = 0–180 min, membrane dose = 7 g L^{-1}, and at room temperature	EBT at pH 5.0 and MG at pH 8.0, with degradation efficiencies of 90.8% and 97.9% under visible light, and 83% and 90% under UV light, respectively	This study

and 633 nm, respectively, and their intensity decreased with the reaction time, as a result of redox processes occurring on the catalyst surface.[63] It was discovered that the CGe–GOgD 30% nanomembrane degraded more rapidly. Additionally, a variety of factors, including the distinct charge separation, shape, and crystallinity of the generated products, affected the rate of dye degradation. Furthermore, a simplified pseudo-first-order (PFO) kinetic model based on the Langmuir–Hinshelwood mechanism was used to calculate the observable rate constant of the dye decomposition procedure. This can be found using the following formula, in which k is the reaction rate constant in minutes, t is the degradation time in minutes, and C is the dye concentration in mg L^{-1}:[64]

$$\ln C_t/C_0 = -kt. \quad (5)$$

Fig. 8(e and f) plot $\ln(C_t/C_0)$ against radiation time for the degradation of EBT and MG dyes using all the synthesized membranes. The apparent first-order rate constant (k) values were used to assess the activity of photocatalysts. A catalyst's performance will increase with a higher value of k. The variance in k values for each of the MG and EBT dyes is shown in Fig. 8(f). For EBT and MG dyes, the correlation coefficient values (R^2) were 0.96 and 0.93, respectively (Fig. 8(f)). The CGe–GOgD 30% nanomembrane had the highest photocatalytic efficiency, and the best photocatalytic performance was achieved with k values of 0.0111 and 0.0129 min^{-1} for EBT and MG, respectively. The CGe–GOgD 30% nanomembrane had the highest photocatalytic efficiency, and the best photocatalytic performance was achieved with k values of 0.0111 and 0.0129 min^{-1} for EBT and MG, respectively (Table 1).

3.6. Photocatalytic degradation mechanism

The photocatalytic procedure of the CGe–GOgD 30% nanomembrane is clearly shown in Fig. 9(a). To boost the photocatalytic activity, adsorption may increase the concentration of EBT dye molecules over the CGe–GOgD 30% nanomembrane, transporting the dyes closer to the surface of the photocatalytic membrane that contains the GogD 30% nanomembrane integrated into the Cge matrix (Fig. 9(a(I))). The production of oxidative species might be initiated by exposing the CGe–GOgD 30% membrane to visible light. Photo-excitation is the process that generates electrons in the conduction band (e^-/CB) and holes in the valence band (h^+/VB), which creates an e^-/h^+ pair. Hydroxyl radicals ($^{\bullet}OH$) are produced when the holes photoreduce the water molecules (H_2O), whereas superoxide radicals ($^{\bullet}O_2$) are produced when the generated electrons combine with the dissolved oxygen (O_2). Both $^{\bullet}OH$ and $^{\bullet}O_2^-$ are highly oxidizing species (Fig. 9(a(II))). In the end, the EBT dye degradation process starts when the radicals $^{\bullet}OH$ and $^{\bullet}O_2^-$ decompose the EBT molecules, generating CO_2 and H_2O as reaction byproducts (Fig. 9(a(III))).

The photocatalytic degradation mechanism of MG and EBT dyes over the Cge–GogD 30% nanomembrane is proposed based on the established photocatalytic processes reported in the literature. Upon irradiation with UV or visible light, the photocatalyst is expected to absorb photons, leading to the excitation of electrons (e^-) from the valence band (VB) to the conduction band (CB), thereby generating electron–hole (e^-/h^+) pairs. The photogenerated holes (h^+) may react with water molecules or hydroxide ions to produce hydroxyl radicals ($^{\bullet}OH$), while the excited electrons (e^-) in the CB can reduce dissolved oxygen to form superoxide radicals ($^{\bullet}O_2^-$). These reactive

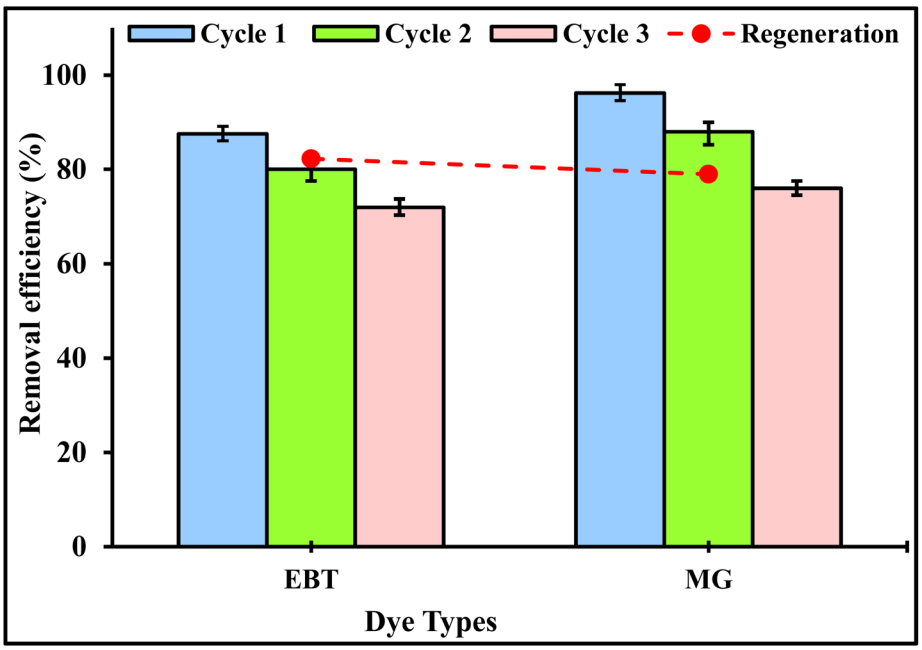

Fig. 10 Recyclability of the CGe–GOgD 30% nanomembrane for the photocatalytic degradation of the EBT and MG dyes at room temperature, pH = 5 for EBT and pH = 8 for MG, contact time = 180 min, dye concentration = 10 mg L^{-1}, and adsorbent dose = 7 g L^{-1}.

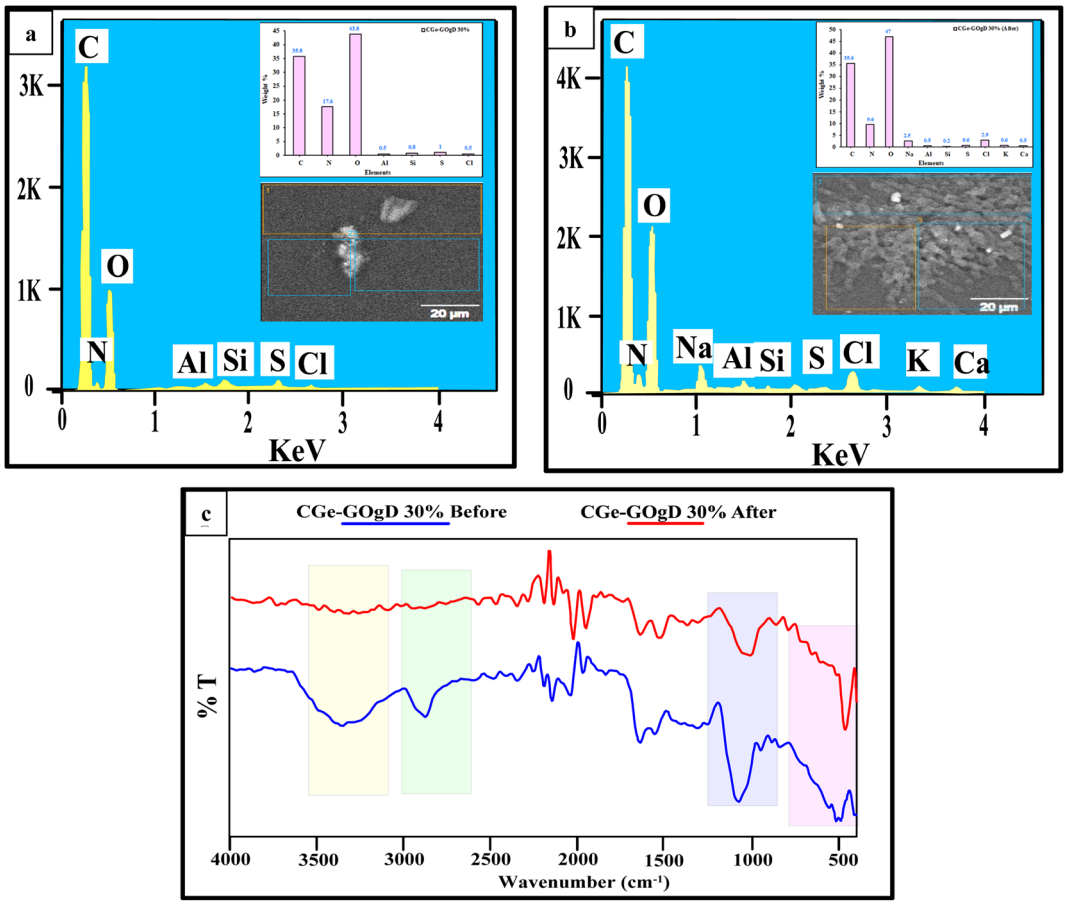

Fig. 11 (a and b) SEM/EDX spectra and (c) FTIR spectra before and after photocatalytic degradation using the CGe–GOgD 30% nanomembrane. Experimental conditions: 10 mg L^{-1} of the MG dye was adsorbed at room temperature for a contact time of 180 min and an adsorbent dose of 7 g L^{-1}.

oxygen species may further undergo a series of reactions, generating additional oxidative species such as hydrogen peroxide (H_2O_2) and hydroxyl radicals.

These highly reactive species ($^{\bullet}OH$, $^{\bullet}O_2^-$, h^+, and e^-) are believed to play a key role in the degradation and mineralization of MG and EBT dyes into CO_2 and H_2O. It should be noted that the proposed mechanism is based on previously reported studies and established photocatalytic behavior.[57]

$$\text{CGe–GOgD 30\% + visible light radiation } (h\nu\text{B}) \rightarrow e^- + h^+, \quad (6)$$

$$O_2 + e^- \rightarrow {}^{\bullet}O_2^-, \quad (7)$$

$$^{\bullet}O_2^- + H^+ \rightarrow HO_2^{\bullet}, \quad (8)$$

$$HO_2^{\bullet} + e^- + H^+ \rightarrow H_2O_2, \quad (9)$$

$$H_2O_2 + {}^{\bullet}O_2^- \rightarrow {}^{\bullet}OH + H^+, \quad (10)$$

$$h^+ + H_2O \rightarrow H^+ + {}^{\bullet}OH, \quad (11)$$

$$h^+ + OH^- \rightarrow {}^{\bullet}OH, \quad (12)$$

$$^{\bullet}O_2^-, {}^{\bullet}OH, h^+, e^- + \text{MG and EBT dyes} \rightarrow \text{degradation products } (CO_2 + H_2O). \quad (13)$$

To gain direct insights into the main active species, scavenger experiments were conducted utilizing specialized quenchers such as ethylenediaminetetraacetic acid (EDTA), isopropanol (IPA), and benzoquinone (BQ) for h^+, $^{\bullet}OH$, and $^{\bullet}O_2^-$, respectively[65] (Fig. 9(b)). To identify the reactive oxygen species that regulate the catalytic action, the effects of several scavengers on the photo-degradation of the CGe–GOgD 30% membrane under visible light irradiation were investigated. Superoxide radicals ($^{\bullet}O_2^-$) are anticipated to play a major role in the degradation process due to effective electron transfer from the conduction band to dissolved oxygen, as demonstrated by the photocatalytic behavior of the CGe–GOgD 30% nanomembrane under visible light. While photogenerated holes (h^+) play a very minor but non-negligible role, hydroxyl radicals ($^{\bullet}OH$) are probably produced as secondary reactive species through subsequent reactions and contribute to additional oxidation of the EBT dye molecules. Thus, the scavenger's primary order is as follows: $^{\bullet}O_2^- > {}^{\bullet}OH > h^+$.

For the degradation of MG and EBT dyes under visible light, Table 2 compares the photocatalytic efficiency of the CGe–

Table 3 Characteristics of a real textile wastewater sample before and after photocatalytic treatment and rejection using the CGe–GOgD 30% nanomembrane

Variables	Units	Treatment		
		Before	After	R (%)
pH	—	3.84	5.6	—
EC	mS cm^{-1}	22.3	22	1.3
TOC	mg L^{-1}	0.504	0.013	97.4
Al^{3+}		0.04	0.013	67.5
Cr^{2+}		12.405	4.773	61.5
Cu^{2+}		0.04	0.022	45
Fe^{2+}		0.289	0.054	81.3
Mn^{2+}		0.373	0.192	48.5
Ni^{2+}		0.009	0.003	66.7
Pb^{2+}		0.002	0.001	50
Si^{4+}		89.437	29.104	67.5
Sr^{2+}		0.422	0.118	72
V^{5+}		0.282	0.028	90.1
Zn^{2+}		2.668	1.05	60.6
Color	nm	2.508	0.433	82.7

GOgD 30% nanomembrane with different GO systems reported in the literature. It was noticed from the table that the CGe–GOgD 30% nanomembrane had the highest photocatalytic effectiveness under visible light as compared to other adsorbents, regardless of the membrane composition and experimental conditions.

3.6.1. Reusability and regeneration of the CGe–GOgD 30% membrane. The efficacy of the EBT and MG dyes using the CGe–GOgD 30% nanomembrane decreased after three cycles (Fig. 10). The results showed that the nanomembrane under visible light irradiation continued to have a higher efficiency even after three cycles. The regeneration rates for EBT and MG dyes using CGe–GOgD 30% were 82.2% and 79%, respectively. This suggested that the nanomembrane had a high capacity for reuse, reduced operating costs, was advantageous in industry, and could treat sewage at least three times using different anionic and cationic dyes. The remarkable durability of the produced CGe–GOgD 30% nanomembrane, which allowed it to separate the membrane without losing weight after each cycle, can be used to explain this outcome. The high stability and repeatability of the synthesized CGe–GOgD 30% nanomembrane for the photocatalytic degradation of industrial wastewater were also evident from the reusability studies.

3.7. SEM/EDX examination and FTIR analysis of the CGe–GOgD 30% nanomembrane before and after the photocatalytic degradation of dyes

The SEM/EDX analysis of CGe–GOgD 30% before and after use in the photocatalytic degradation of MG dyes (third cycles) is shown in Fig. 11(a and b). Strong surface connections and structure modifications associated with MG dye degradation are further supported by SEM and EDX investigations (Fig. 11(a and b)). Only apparent peaks associated with C, O, N, Al, Si, Cl, and S were found prior to adsorption; however, following the exposure of CGe–GOgD 30% to the photocatalytic degradation of MG dyes, the intensity of these elements increases, and some signals associated with Ca, Na, and K, as well as partially locked surface pores, are detected. Surface alteration and contamination buildup are confirmed by these morphological structure changes. Dye adsorption and subsequent degradation were clearly demonstrated by the FTIR spectra of the CGe–GOgD 30% membrane, which were confirmed both before and after the photocatalytic destruction of the MG dye under visible light (Fig. 11(c)). The CGe–GOgD 30% nanomembrane ingredients' typical peaks can be seen in the spectrum prior to photocatalytic degradation. A large absorption band at 3200–3400 cm^{-1} is attributed to the O–H and N–H stretching vibrations from chitosan/gelatin, D, and GO. The amide I and amide II bands of CGe–GOgD 30% were represented by the bands found at 1650 and 1540 cm^{-1}, while the peaks seen at 1100–1250 cm^{-1} were attributed to the stretching vibrations of GO and the polymer backbone. When MG dyes were present, the noticeable band intensity changed, and minor peak shifts were seen, especially in the O–H/N–H and aromatic C=C regions at 1500–1600 cm^{-1}. These changes indicated a strong interaction between the MG

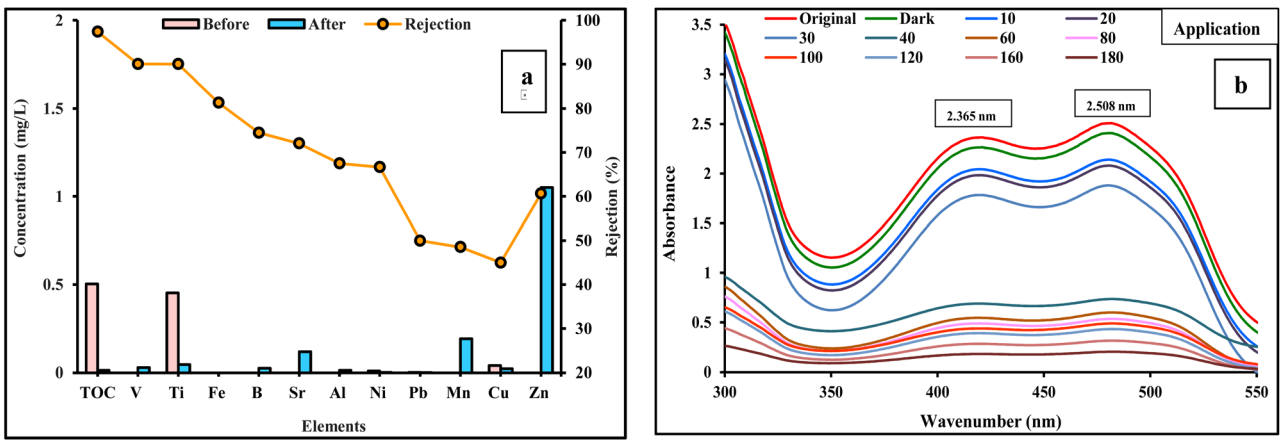

Fig. 12 (a) Photocatalytic treatment of an actual textile wastewater sample using CGe–GOgD 30% before and after, with the R% values. (b) UV-visible spectra of the degradation with time.

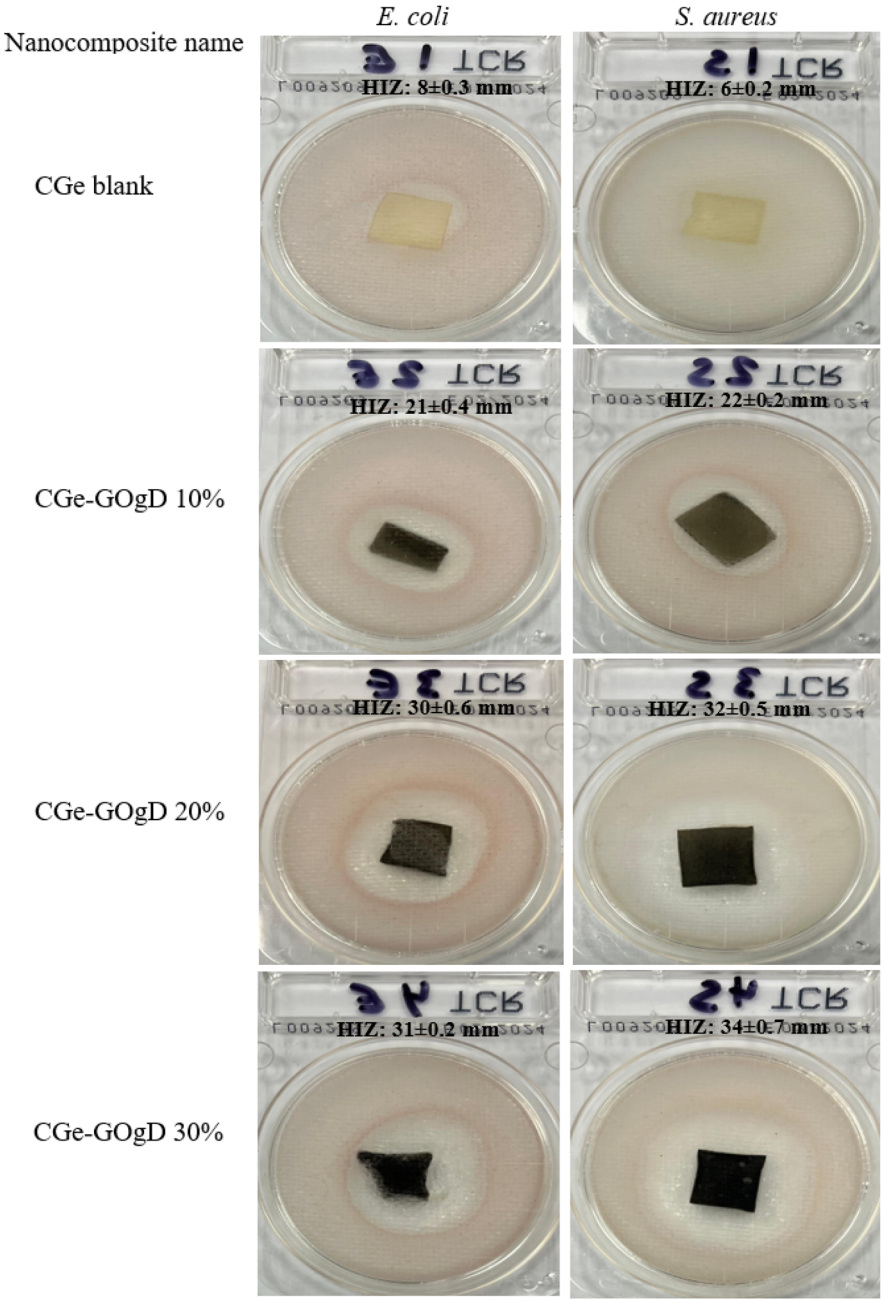

Fig. 13 Antibacterial experiments and inhibitory zones of the CGe blank and the nanomembranes with different ratios of GOgD against the *E. coli* and *S. aureus* bacteria.

dye molecules and the functional sites of the CGe–GOgD 30% nanomembrane. Moreover, operative photocatalytic degradation, as opposed to the straightforward physical adsorption, was shown by the decrease or elimination of distinctive MG-associated bands. These spectrum shifts demonstrated the connection between surface amine, aromatic, and hydroxyl groups in the degradation mechanism and validated the function of GOgD as an active visible light photocatalyst. The asymmetrical vibrations of the stretching of aliphatic C–H (–CH_2/–CH_3) groups generated by the D structure and polymeric framework were responsible for the absorption band appearing at 2876 cm^{-1}. Variations in its intensity during photocatalytic treatment demonstrate surface interactions and structural alterations that coincide with the degradation of MG dye.

3.8. Using the CGe–GOgD 30% nanomembrane to an industrial wastewater sample

It was examined how the generated CGe–GOgD 30% nanomembrane affected the actual wastewater's photocatalytic activity. There is a noticeable drop in color and elements in Fig. 12 and Table 3. The CGe–GOgD 30% nanomembrane improved color removal, which dropped from 2.508 to 0.433 nm

with an 82.7% rejection rate, suggesting a noticeably lower concentration (Table 3). This displayed the effectiveness of the CGe–GOgD 30% nanomembrane as a photocatalytic invention. The findings showed that the EC (mS cm^{-1}) dropped from 22.3 to 22, and the pH improved from 3.84 to 5.6. With rejection equal to 97.4%, Table 3 shows that the textile wastewater's TOC had dropped from 0.504% to 0.013%. Additionally, the CGe–GOgD 30% nanomembrane had a good removal efficiency for both organic dyes and several hazardous heavy metals (Table 3). As seen in Fig. 12(b), the actual wastewater sample likewise showed photocatalytic deterioration over time. The enhanced nanomembranes' better purifying water capability allowed for the production of superior water at a lower cost. They also showed strong chemical and mechanical strength. Therefore, it is necessary to develop and construct the CGe–GOgD 30% nanomembrane, complying with the standards appropriate for industrial usage, and its performance should be compared to products that are available on both domestic and foreign markets. Therefore, its properties ought to be beneficial for the elimination of salts, heavy metal ions, and organic molecules (dyes) from saline wastewater. A shift from the initial adsorption-dependent stage to a more effective photocatalytic decomposition phase is shown by the discernible drop in absorbance intensity between 30 and 40 min (Fig. 12(b)). Dye molecules are mainly adsorbed onto the CGe–GOgD 30% nanomembrane surface during the early irradiation period (up to 30 min), accompanied by partial degradation, which causes a steady decrease in absorbance. After this time, the system enters a key activation stage where enough reactive oxygen species (such $^{\bullet}OH$ and $^{\bullet}O_2^-$ radicals) are produced, causing the dye optical complexes to break down quickly and the absorbance to decrease significantly. This behavior validates the beneficial interaction of adsorption and photocatalysis in increasing the dye elimination efficiency and corresponds to the typical two-stage kinetics of photocatalytic systems, where an induction period is followed by accelerated degradation.

3.9. Antibacterial screening

The antibacterial activity of the unfilled blend and the nanomembranes containing variable GOgD contents was evaluated to assess the potential of these nanomembranes for eliminating biological contaminants from wastewater. The experiment was assessed using two different bacteria, *E. coli* and *S. aureus*, at a contact time of 24 h and at 37 °C (Fig. 13). The figure demonstrated that the unfilled CGe film had a slight inhibitory effect on the two selected microbes used in the test. This suggested the biological activity of the CGe matrix.[74] With the incorporation of GOgD into the matrix, clear halos of inhibition were noticed for all nanomembranes loaded with GOgD of different diameters ranging from 21 mm to 34 mm, depending on the type of bacteria and nanomembrane. This improvement was associated with the presence of active sites in dapsone, such as amino and sulfonyl (O═S═O), besides the barrier property of GO, which had a significant impact on repressing the growth of a wide spectrum of G^{-ve} and G^{+ve} bacteria.[25,75,76] Surprisingly, the data also showed that the highest antibacterial activity *versus* the two selected microbes was achieved at a higher dosage of GOgD (*i.e.* 30%). Thus, the antibacterial mechanism can be rounded-up as follows: a further increase in the content of dapsone molecules in the matrix enhanced their ability to adhere to the bacterial cytoplasm and cell wall, thereby inhibiting microbial growth.[27,77] Additionally, it has been previously demonstrated in the literature[78,79] that the electrostatic interactions between the functional sites on the nanomembrane and the anionic groups on bacterial surfaces could lead to the damage of the cell membrane of the microbes, further contributing to antibacterial activity. Therefore, GO grafting by D is influential, and the utilization of CGe–GOgD nanomembranes is considered to be a promising strategy for the removal of toxic dyes and biological pollutants from wastewater.

4. Conclusions

In the current work, green and efficient nanomembranes were successfully prepared by grafting GO using benign dapsone (D) to improve the properties of CGe nanomembranes. The chemical structure of grafted GOgD nanoplatelets was investigated using the FT-IR spectra, XRD patterns, and Raman spectra. Three varying dosages of GOgD (10–30%) were utilized to prepare the nanomembranes by using a solvent-casting procedure. A series of investigations and measurements, including morphology, mechanical properties, photocatalytic performance, and antibacterial activities, were applied to characterize the CGe nanocomposites. The mechanical outcomes showed that the best enhancement was achieved for tensile strength at 20%, and was found to be ~85 MPa compared to the CGe blank (61.35 MPa). Otherwise, a high GOgD dosage (30%) can lead to obtaining nanofiller aggregations. This was confirmed by SEM observations. CGe nanomembranes based on GogD showed strong antibacterial activities against G^{-ve} and G^{+ve} bacteria, as compared to the blank matrix. Photocatalytic experiments were conducted using UV and visible light. The obtained data revealed that the photocatalytic degradation occurred in the following order: CGe–GOgD 30% > CGe–GOgD 20% > CGe–GOgD 10% > pure CGe. Under visible light, the CGe–GOgD 30% nanomembrane achieved higher removal efficiencies of 90.8% and 97.9% for EBT and MG, respectively, and 83% and 90% under UV light. The CGe–GOgD 30% nanomembrane exhibited excellent visible light energetic photocatalytic activity with optimal performance at pH 5 for EBT and pH 8 for MG. For MG and EBT dyes, a progressive decline in degradation efficiency was noted as the initial dye concentration and the contact duration increased. The results also showed that the CGe–GOgD 30% nanomembrane under visible light continued to have a higher efficiency even after three cycles, with regeneration rates of 82.2% and 79% for EBT and MG dyes, respectively. The application of the CGe–GOgD 30% nanomembrane to an industrial wastewater sample resulted in a significant improvement in color removal, dropping the absorbance from 2.508 to 0.433 nm and achieving an 82.7% rejection rate. This innovative integrated system not only eliminates the adverse environmental impacts associated with textile effluents but also

supplies ample freshwater for use in industry, agriculture, and landscaping.

Conflicts of interest

The authors declare that there is no conflict of interest in the work.

Data availability

The authors confirm that the data supporting the results of this study are available within the article.

Acknowledgements

This work was supported and funded by the Deanship of Scientific Research at Imam Mohammad Ibn Saud Islamic University (IMSIU) (grant number IMSIU-DDRSP2602).

References

1 S. S., Medha and S. Thakur, *Mater. Today: Proc.*, 2023, **78**, 815–824.
2 T. Biswal, T. R. Sethy and P. K. Sahoo, *ACS Symp. Ser.*, 2024, **1486**, 197–214.
3 M. Z. Alam, M. N. Bari and S. Kawsari, *Environ. Sustain. Indic.*, 2022, **14**, 100176.
4 R. Al-Tohamy, S. S. Ali, F. Li, K. M. Okasha, Y. A. G. Mahmoud, T. Elsamahy, H. Jiao, Y. Fu and J. Sun, *Ecotoxicol. Environ. Saf.*, 2022, **231**, 113160.
5 W. J. Ong, L. L. Tan, Y. H. Ng, S. T. Yong and S. P. Chai, *Chem. Rev.*, 2016, **116**, 7159–7329.
6 A. Kaur, S. Kumar, H. Kaur, G. S. Lotey, P. P. Singh, G. Singh, N. Supreet, S. Kumar, J. Dalal, G. Bouzid, M. Misra, R. Pandey and S. Kaushal, *Mater. Adv.*, 2024, **5**, 8111–8131.
7 N. Kaur, M. Bansal, P. Kaur, K. Kaur, A. Awasthi, S. K. Nippani, S. Das and A. Lodh, *Front. Environ. Sci.*, 2025, **13**, 1656031.
8 A. Tkaczyk, K. Mitrowska and A. Posyniak, *Sci. Total Environ.*, 2020, **717**, 137222.
9 M. Ismail, K. Akhtar, M. I. Khan, T. Kamal, M. A. Khan, A. M. Asiri, J. Seo and S. B. Khan, *Curr. Pharm. Des.*, 2019, **25**, 3645–3663.
10 J. C. Maxwell, B. C. Baker and C. F. J. Faul, *ACS Appl. Polym. Mater.*, 2023, **5**, 662–671.
11 M. C. Danner, A. Robertson, V. Behrends and J. Reiss, *Sci. Total Environ.*, 2019, **664**, 793–804.
12 K. O. Imwene, E. Ngumba and P. K. Kairigo, *J. Environ. Manage.*, 2022, **322**, 116065.
13 A. S. Oberoi, Y. Jia, H. Zhang, S. K. Khanal and H. Lu, *Environ. Sci. Technol.*, 2019, **53**, 7234–7264.
14 D. M. Montoya-Rodríguez, E. A. Serna-Galvis, F. Ferraro and R. A. Torres-Palma, *J. Environ. Manage.*, 2020, **261**, 110224.
15 A. Champati, P. K. Sahu, A. Rath, B. Naik and A. Pradhan, *ACS Omega*, 2025, **10**, 43871.
16 T. B. Mbuyazi and P. A. Ajibade, *Int. J. Mol. Sci.*, 2024, **25**, 7876.
17 I. Badran and M. O. Al-Ejli, *Mater. Today Commun.*, 2024, **41**, 110302.
18 I. De, M. Pahuja, H. M. ud din Wani, A. Dey, T. Dube, R. Ghosh, N. Kankan, J. Mishra, J. J. Panda, T. Maruyama, K. Ghosh and M. Singh, *Ecotoxicol. Environ. Saf.*, 2022, **243**, 113985.
19 H. Moustafa, M. H. Hemida, M. A. Shemis, A. Dufresne and M. Morsy, *Surf. Interfaces*, 2023, **41**, 103229.
20 H. Moustafa, M. Morsy, M. A. Ateia and F. M. Abdel-Haleem, *Sens. Actuators, A*, 2021, **331**, 112918.
21 W. A. Al-Masoudi, T. M. Al-Tememy and R. H. Al-Assadi, *Eur. J. Chem.*, 2014, **5**, 351–355.
22 G. G. Zhanel and J. Q. Del Rosso, *Journal of Clinical and Aesthetic Dermatology*, 2016, **9**, 42.
23 V. E. G. Wozel, *Dermatol. Clin.*, 2010, **28**, 599–610.
24 A. Chakraborty, A. K. Panda, R. Ghosh and A. Biswas, *Arch. Biochem. Biophys.*, 2019, **665**, 107–113.
25 H. Moustafa, M. A. Shemis, E. M. Ahmed and H. Isawi, *RSC Adv.*, 2024, **14**, 19680–19700.
26 H. Isawi, E. M. Ahmed, M. Rabee and H. Moustafa, *J. Ind. Eng. Chem.*, 2024, **141**, 626–644.
27 H. Moustafa, A. M. Karmalawi and A. M. Youssef, *Environ. Nanotechnol. Monit. Manag.*, 2021, **16**, 100482.
28 H. Moustafa, S. Fawzy Ibrahim, E. M. Ahmed and H. Atef, *J. Vinyl Addit. Technol.*, 2024, **30**, 855–867.
29 M. Nurilmala, H. Suryamarevita, H. Husein Hizbullah, A. M. Jacoeb and Y. Ochiai, *Saudi J. Biol. Sci.*, 2022, **29**, 1100–1110.
30 W. M. Saleh, E. B. Yahya, M. I. Ahmad and H. P. S. A. Khalil, *Polym. Eng. Sci.*, 2024, **64**, 3993–4001.
31 V. Venezia, M. Verrillo, P. R. Avallone, B. Silvestri, S. Cangemi, R. Pasquino, N. Grizzuti, R. Spaccini and G. Luciani, *Biomacromolecules*, 2023, **24**, 2691–2705.
32 T. Sarwar, Z. A. Raza, M. A. Nazeer and A. Khan, *Int. J. Biol. Macromol.*, 2023, **253**, 126588.
33 M. Chelu, A. M. Musuc, M. Popa and J. M. Calderon Moreno, *Gels*, 2023, **9**, 664.
34 I. Choi, B. Y. Lee, S. Kim, S. Imm, Y. Chang and J. Han, *Food Sci. Biotechnol.*, 2023, **32**, 1067.
35 J. M. Queirós, F. Zheng, R. Brito-Pereira, M. M. Fernandes, E. O. Carvalho, P. M. Martins, V. Lazić, J. M. Nedeljković and S. Lanceros-Mendez, *RSC Sustain.*, 2025, **3**, 4568–4582.
36 J. Liu, S. Wang, K. Xu, Z. Fan, P. Wang, Z. Xu, X. Ren, S. Hu and Z. Gao, *Carbohydr. Polym.*, 2020, **236**, 115963.
37 K. Kaur and R. Jindal, *Carbohydr. Polym.*, 2019, **207**, 398–410.
38 S. Ahmed and S. Ikram, *J. Photochem. Photobiol., B*, 2016, **163**, 115–124.
39 H. Moustafa, N. A. Darwish, A. M. Youssef, S. M. Reda, A. El-Aziz and A. El-Wakil, *Egypt. J. Chem.*, 2018, **21**, 23–32.
40 H. Moustafa, E. M. Ahmed, M. Hemida, M. Rabee and H. Isawi, *Diamond Relat. Mater.*, 2025, **157**, 112552.
41 H. Moustafa, S. Duquesne, B. Haidar and M. F. F. Vallat, *Polym. Compos.*, 2017, **38**, 966–973.
42 H. Isawi, *Chem. Eng. Process.*, 2023, **187**, 109343.
43 Mohamed Morsy, A. I. Abdel-Salam, H. Moustafa and I. Gomaa, *Molecules*, 2023, **28**, 108.

44 F. M. Abdel-Haleem, M. Hemida and H. Moustafa, *J. Adhes. Sci. Technol.*, 2025, **39**, 3099–3115.
45 H. Moustafa, F. M. Abdel-Haleem and M. H. Hemida, *RSC Adv.*, 2026, **16**, 11496–11505.
46 M. Yadav, S. Ahmad and F. C. Chiu, *J. Ind. Eng. Chem.*, 2018, **68**, 246–256.
47 J. Brzeska, A. Maria, E. Id, M. Morawska, W. Sikorska, M. Kowalczuk and M. Rutkowska, *Polymers*, 2021, **13**, 1202.
48 E. O. Cisneros-López, M. E. González-López, A. A. Pérez-Fonseca, R. González-Núñez, D. Rodrigue and J. R. Robledo-Ortíz, *Compos. Interfaces*, 2017, **24**, 35–53.
49 M. Shemis, H. Moustafa, F. H. Salman, G. Safwat, M. Moharib and S. Mamdouh, *Next Research*, 2026, **5**, 101368.
50 F. T. Johra, J. W. Lee and W. G. Jung, *J. Ind. Eng. Chem.*, 2014, **20**, 2883–2887.
51 M. Kasztelan, A. Słoniewska, M. Gorzkowski, A. Lewera, B. Pałys and S. Zoladek, *Appl. Surf. Sci.*, 2021, **554**, 149060.
52 H. Nagahama, H. Maeda, T. Kashiki, R. Jayakumar, T. Furuike and H. Tamura, *Carbohydr. Polym.*, 2009, **76**, 255–260.
53 W. Ding, S. Guo, K. Wang, X. Pang, B. S. Asres and Z. Ding, *Int. J. Biol. Macromol.*, 2025, **284**, 138104.
54 S. Akel, R. Boughaled, R. Dillert, M. El Azzouzi and D. W. Bahnemann, *Molecules*, 2020, **25**, 249.
55 P. Bhattacharya and S. Chakravorti, *Chem. Phys. Lett.*, 2013, **571**, 71–76.
56 R. A. El-Kholy, H. Isawi, E. Zaghlool, E. A. Soliman, M. M. H. Khalil, M. M. Said, A. elhameed and M. El-Aassar, *Environ. Sci. Pollut. Res.*, 2023, **30**, 69514–69532.
57 H. M. Abomostafa, H. Isawi, D. E. Abulyazied and A. S. Abouhaswa, *Surf. Interfaces*, 2023, **42**, 103402.
58 S. Elbakry, M. E. A. Ali, M. Abouelfadl, N. A. Badway and K. M. M. Salam, *J. Photochem. Photobiol., A*, 2022, **430**, 113957.
59 S. Nayak, T. M. Subrahmanya, S. H. Abebe, H. Chi-Ying, H. F. M. Austria, R. D. H. T. Cayron, W. S. Hung, C. C. Hu and J. Y. Lai, *Sep. Purif. Technol.*, 2025, **372**, 133512.
60 H. Isawi, *Arabian J. Chem.*, 2020, **13**, 5691–5716.
61 D. Singh, K. M. Batoo, S. Hussain, A. Kumar, Q. H. Aziz, F. S. Sheri, H. Tariq and P. Singh, *RSC Adv.*, 2024, **14**, 2429–2438.
62 A. K. Tolkou, I. A. Katsoyiannis and G. Z. Kyzas, *J. Compos. Sci.*, 2025, **9**, 327.
63 N. Pourshirband and A. Nezamzadeh-Ejhieh, *Mater. Res. Bull.*, 2022, **148**, 111689.
64 N. M. Dat, P. N. B. Long, D. C. U. Nhi, N. N. Minh, L. M. Duy, L. N. Quan, H. M. Nam, M. T. Phong and N. H. Hieu, *Synth. Met.*, 2020, **260**, 116260.
65 A. Zhu, L. Qiao, Z. Jia, P. Tan, Y. Liu, Y. Ma and J. Pan, *Dalton Trans.*, 2017, **46**, 17032–17040.
66 H. Chi, P. Cao, Q. Shi, C. Song, Y. Lv and T. Peng, *Nanomaterials*, 2025, **15**, 383.
67 Z. Shen, J. Shi, L. Xiao, B. Yu, X. Chen and C. Zhang, *Mater. Res. Bull.*, 2026, **196**, 113925.
68 R. P. Dhavale, V. D. Phadtare, S. A. Chaudhari, M. G. Mali, V. G. Parale, S. V. Mohite, D. Lee, H. Choi, A. A. Ransing, J. Kim, S. H. Kim, P. B. Patil, J. C. Pyun and H. H. Park, *J. Water Proc. Eng.*, 2026, **83**, 109591.
69 P. Makal and D. Das, *J. Environ. Chem. Eng.*, 2019, **7**, 103358.
70 R. Khurram, A. Javed, R. Ke, C. Lena and Z. Wang, *Nanomaterials*, 2021, **11**, 2021.
71 A. M. Ismael, A. N. El-Shazly, S. E. Gaber, M. M. Rashad, A. H. Kamel and S. S. M. Hassan, *RSC Adv.*, 2020, **10**, 34806–34814.
72 P. Parthenidis, K. N. Maroulas, E. Evgenidou, G. Z. Kyzas and D. A. Lambropoulou, *J. Water Proc. Eng.*, 2025, **74**, 107824.
73 T. D. Kusworo, A. C. Kumoro, N. Aryanti, H. Hasbullah, D. R. S. Chaesarifa, M. D. Fauzan and F. Dalanta, *J. Environ. Chem. Eng.*, 2023, **11**, 109449.
74 C. Wang, B. Wang, X. Ji, X. Tang, Y. Li, Y. Huang and X. Ma, *Int. J. Biol. Macromol.*, 2025, **319**, 145488.
75 L. H. do Amaral, F. A. do Carmo, M. I. Amaro, V. P. de Sousa, L. C. R. P. da Silva, G. S. de Almeida, C. R. Rodrigues, A. M. Healy and L. M. Cabral, *AAPS PharmSciTech*, 2018, **19**, 2687–2699.
76 A. Madbouly, M. Morsy and H. Moustafa, *Ceram. Int.*, 2024, **50**, 38522–38531.
77 D. L. Williams, T. Hagino, R. Sharma and D. Scollard, *Emerg. Infect. Dis.*, 2013, **19**, 179–180.
78 W. Yang, J. S. Owczarek, E. Fortunati, M. Kozanecki, A. Mazzaglia, G. M. Balestra, J. M. Kenny, L. Torre and D. Puglia, *Ind. Crops Prod.*, 2016, **94**, 800–811.
79 E. Robles, A. M. Salaberria, R. Herrera, S. C. M. Fernandes and J. Labidi, *Carbohydr. Polym.*, 2016, **144**, 41–49.